

# Bayesian modeling of nearly mutually orthogonal processes

James Matuk<sup>1</sup>, Amy H. Herring<sup>1,2,3</sup>, and David B. Dunson<sup>1,4</sup>

<sup>1</sup>Department of Statistical Science, Duke University, Durham, NC, USA

<sup>2</sup>Duke Global Health Institute, Duke University, Durham, NC, USA

<sup>3</sup>Department of Biostatistics and Bioinformatics, Duke University,  
Durham, NC, USA

<sup>4</sup>Department of Mathematics, Duke University, Durham, NC, USA

## Abstract

Functional factor analysis is an important dimension reduction method for functional and longitudinal data. Factor loadings give insight into patterns of variability of the observations, while latent factors provide a low-dimensional representation of the data that is useful for inferential tasks. Constraining the functional factor loadings to be mutually orthogonal is desirable for model parsimony, but is computationally challenging. In this work, we introduce nearly mutually orthogonal processes, which can be used to effectively enforce mutual orthogonality of the factor loadings, while maintaining computational simplicity and efficiency. The joint distribution is governed by a penalty parameter that determines the degree to which the processes are mutually orthogonal and is related to ease of posterior computation. We demonstrate that our approach can be used for flexible and interpretable inference in an application to studying the effects of breastfeeding status, illness, and demographic factors on weight dynamics in early childhood. Code is available on GitHub: <https://github.com/jamesmatuk/NeMO-FFA>

*Keywords:* Bayes; Functional data analysis; Gaussian process; Orthogonality; Uncertainty quantification.

# 1 Introduction

The ability to encode constraints into Bayesian nonparametric regression models is important for posterior inference that is consistent with prior knowledge. There is a rich literature on constrained Bayesian nonparametric regression focused on monotonicity (Shively et al. 2009, Lin & Dunson 2014), convexity or concavity (Shively et al. 2011, Hannah & Dunson 2013, Lenk & Choi 2017), and other shape constraints (Wheeler et al. 2017, Dasgupta et al. 2021, Yu et al. 2022). In this work we seek to enforce a relaxed version of a mutual orthogonality constraint for functional parameters. To this end, we define nearly mutually orthogonal (NeMO) processes. The joint distribution induced by NeMO processes is governed by a penalty parameter controlling departures from mutual orthogonality, similar in spirit to the Bayesian constraint relaxation framework of Duan et al. (2019). While orthogonality plays an important role in many areas, such as semiparametric inference (Plumlee & Joseph 2018, Kowal & Canale 2021) and modeling spatial random effects (Hodges & Reich 2010, Khan & Calder 2022), we motivate NeMO processes through applications to factor analysis of functional data.

A fundamental problem in functional data analysis is that observations are generated from infinite-dimensional stochastic processes (Ramsay & Silverman 2005, Ferraty & Vieu 2006). Consequently, dimension reduction is an important modeling tool. Low-dimensional representations of functional data can retain most of the information in the original observations when the modes of variability are assumed to be smooth. Functional factor analysis provides a generative model for functional data that decomposes observations into latent factors and functional factor loadings. The loadings are useful for understanding patterns of variability in the observations, while the latent factors served as a low-dimensional representation of the data. Bayesian hierarchical models are successful in using the latent factors for a variety of inferential tasks, including regression (Montagna et al. 2012), joint modeling (Moran et al. 2021), clustering (Marco et al. 2022), and modeling multivariate functional data (Kowal et al. 2017, Kowal 2021).

The most popular dimension reduction tool for functional data is functional principal component analysis (James et al. 2000, Yao et al. 2005, Peng & Paul 2009). When viewed through a probabilistic framework (Tipping & Bishop 1999), functional principal components are functional factor loadings, while projections of the data onto the components are latent factors. For relevant Bayesian articles, refer to Behseta et al. (2005), van der Linde (2008), Suarez & Ghosal (2017), Jiang et al. (2020), Nolan et al. (2021). Within this context, a mutual orthogonality constraint is imposed on the factor loadings to aid interpretability of latent factors, especially for subsequent inferential tasks. We effectively enforce this constraint by using the NeMO process prior to shrink factor loadings towards mutually orthogonality. Taking an over-fitted factor modeling approach, NeMO effectively deletes unnecessary factors by favoring their loadings to be close to zero. Hence, NeMO represents a fundamentally new strategy for choosing the number of factors, providing an appealing alternative to approaches that define aggressive shrinkage priors for the loadings without the orthogonality constraint (Bhattacharya & Dunson 2011, Schiavon et al. 2022). In contrast to shrinking towards orthogonality, exact orthogonality can be imposed through an appropriate prior as in Jauch et al. (2021), however strictly enforcing mutual orthogonality can lead to computational inefficiency (Shamshoian et al. 2022).

In addition to understanding important properties of NeMO processes as a prior model, we demonstrate that they can serve as a foundation for Bayesian functional factor analysis in a wide range of application settings, including sparse and irregular observations and generalized functional data. We highlight the computational tractability of NeMO processes. The specified probability model for each factor loading is conditionally conjugate for Gaussian likelihoods, which leads to simple posterior computation. Finally, we illustrate how NeMO processes can be used as a layer in a hierarchical model, providing advantages over existing approaches in terms of flexibility, interpretability, computational convenience and uncertainty quantification.

## 2 Nearly Mutually Orthogonal Processes

### 2.1 Definition of Nearly Mutually Orthogonal Processes

We define NeMO processes with the goal of developing a prior model that shrinks the pairwise inner products of a set of random functions,  $\{\lambda_k : \mathcal{T} \rightarrow \mathbb{R}\}_{k=1}^K$ . Our prior enforces a relaxed version of the following mutual orthogonality constraint:

$$\langle \lambda_j, \lambda_k \rangle := \int_{\mathcal{T}} \lambda_j(s) \lambda_k(s) ds = 0, \quad j \neq k, \quad (1)$$

where  $\langle \cdot, \cdot \rangle$  denotes the  $\mathbb{L}^2$  inner product between two functions. Let  $\mathcal{G}$  denote the product measure induced by  $K$  independent zero-mean Gaussian processes with covariance kernels  $C_k(\cdot, \cdot)$ ,  $k = 1, \dots, K$ , and  $\mathcal{H}$  denote the product of reproducing kernel Hilbert spaces defined by the covariance kernels (van Zanten & van der Vaart 2008). We refer to these as *parent Gaussian processes*. We assume the measure induced by NeMO processes, denoted by  $\mathcal{N}$ , is absolutely continuous with respect to  $\mathcal{G}$ . We define  $\mathcal{N}$  through the Radon-Nikodym derivative,

$$\frac{\partial \mathcal{N}}{\partial \mathcal{G}}(\lambda_1, \dots, \lambda_K) \propto \exp \left( - \frac{1}{2\nu_\lambda} \sum_{k=1}^K \sum_{j < k} \langle \lambda_j, \lambda_k \rangle^2 \right). \quad (2)$$

The degree to which the mutual orthogonality constraint is met is governed by the penalty parameter,  $\nu_\lambda$ . The limiting properties of  $\mathcal{N}$  with respect to  $\nu_\lambda$  are summarized by Propositions 2.1 & 2.2.

**Proposition 2.1.** *Let  $E := \{\lambda_1, \dots, \lambda_K \in \mathcal{H} \mid \langle \lambda_j, \lambda_k \rangle \neq 0, \text{ for some } j \neq k\}$ . For any measurable subset  $E' \subseteq E$ ,  $\lim_{\nu_\lambda \rightarrow 0} \mathcal{N}(E') = 0$ .*

**Proposition 2.2.** *For any measurable set  $A \subseteq \mathcal{H}$ ,  $\lim_{\nu_\lambda \rightarrow \infty} \mathcal{N}(A) = \mathcal{G}(A)$ .*

For measurable subsets of non-mutually orthogonal functions,  $E'$ ,  $\mathcal{N}$  has measure zero, as  $\nu_\lambda \rightarrow 0$ . On the other hand, for any measurable set,  $A$ ,  $\mathcal{N}$  is equal in measure to  $\mathcal{G}$ , as  $\nu_\lambda \rightarrow \infty$ . Consequently, for fixed  $\nu_\lambda > 0$ ,  $\mathcal{N}$  balances Gaussian process-like behavior and

mutual orthogonality. As a result, NeMO processes inherit properties from the covariance functions used to define the parent Gaussian processes, such as magnitude, smoothness, and periodicity. The role of these covariance functions is further discussed in Section 2.3.

To study  $\mathcal{N}$  with fixed  $\nu_\lambda > 0$ , we define a set of all functions  $\{\lambda_1, \dots, \lambda_K\}$  that are  $\omega$ -far from being mutually orthogonal:  $E_\omega := \{\lambda_1, \dots, \lambda_K \in \mathcal{H} \mid \sum_1^K \sum_{j < k} \langle \lambda_j, \lambda_k \rangle^2 > \omega\}$ . For increasing  $\omega$ ,  $E_\omega$  will not contain any functions that are close to mutually orthogonal, quantified through the pairwise sum of squared inner products. Proposition 2.3 formalizes the behavior of  $\mathcal{N}$  for measurable subsets of  $E_\omega$ .

**Proposition 2.3.** *For any  $\nu_\lambda > 0$  and measurable subset  $E'_\omega \subseteq E_\omega$  with non-zero  $\mathcal{G}(E'_\omega)$ ,*

$$\frac{\mathcal{N}(E'_\omega)}{\mathcal{G}(E'_\omega)} \leq F \exp\left(-\frac{\omega}{2\nu_\lambda}\right),$$

where  $F = [\mathbb{E}_{\mathcal{G}}\{\exp(-\frac{1}{2\nu_\lambda} \sum_1^K \sum_{j < k} \langle \lambda_j, \lambda_k \rangle^2)\}]^{-1}$  is a normalizing constant.

Relative to the Gaussian measure,  $\mathcal{N}$  assigns probability to  $E'_\omega$  that decays exponentially fast as  $\omega$  increases, with rate governed by  $\frac{1}{2\nu_\lambda}$ . This implies that, relative to drawing  $\lambda_1, \dots, \lambda_K$  independently from Gaussian processes, sampling from a NeMO process will place higher probability on functions that are close to mutually orthogonal.

Proofs for Propositions 2.1, 2.2, and 2.3 are presented in Appendix A.

## 2.2 Conditional Distribution of $\lambda_k$ given $\{\lambda_j\}_{j \neq k}$

Assigning the functional factor loadings a NeMO process prior,  $\{\lambda_1, \dots, \lambda_K\} \sim \mathcal{N}$ , we develop a broad class of methods for functional factor analysis in Section 3. A concern is that posterior computation may be difficult due to the analytically intractable normalizing constant of the measure  $\mathcal{N}$  defined in Equation (2). However, we bypass this problem by exploiting a simple form for the conditional distribution of  $\lambda_k$  given  $\{\lambda_j\}_{j \neq k}$  under the joint prior  $\{\lambda_1, \dots, \lambda_K\} \sim \mathcal{N}$ . This conditional distribution is stated in Proposition 2.4.

**Proposition 2.4.** *Given  $\{\lambda_j\}_{j \neq k}$ ,  $\lambda_k$  is a zero-mean Gaussian process with covariance*

$$C_k^{\nu_\lambda}(s, t) = C_k(s, t) - h_{\Lambda_{(-k)}}(s)^\top \{\nu_\lambda I_{K-1} + H_{\Lambda_{(-k)}}\}^{-1} h_{\Lambda_{(-k)}}(t), \text{ where} \quad (3)$$

$$h_{\Lambda_{(-k)}}(t) = \int_{\mathcal{T}} C_k(s, t) \Lambda_{(-k)}(s) ds, \quad H_{\Lambda_{(-k)}} = \int_{\mathcal{T}} \int_{\mathcal{T}} C_k(s, s') \Lambda_{(-k)}(s) \Lambda_{(-k)}(s')^\top ds ds' \quad (4)$$

with  $\Lambda_{(-k)}(s) = \{\lambda_1(s), \dots, \lambda_{k-1}(s), \lambda_{k+1}(s), \dots, \lambda_K(s)\}^\top$ .

Proposition 2.4 implies that the finite-dimensional conditional distribution of  $\lambda_k$  evaluated at a fixed set of points, given  $\{\lambda_j\}_{j \neq k}$ , is multivariate Gaussian, which is conditionally conjugate to the Gaussian likelihood of discretely observed functional data assumed in the model in Section 3. Conditional conjugacy enables posterior inference through a computationally simple Gibbs sampler, outlined in Section 3.4. The behavior of  $\lambda_k \mid \{\lambda_j\}_{j \neq k} \sim \text{GP}\{0, C_k^{\nu_\lambda}(\cdot, \cdot)\}$  is governed by the covariance function  $C_k^{\nu_\lambda}(s, t) = \text{cov}\{\lambda_k(s), \lambda_k(t) \mid \{\lambda_j\}_{j \neq k}\}$ , illustrated in Section 2.3.

Conditionally, NeMO processes are related to the orthogonal Gaussian processes of Plumlee & Joseph (2018), introduced in the context of design and analysis of computer experiments. Their goal was to develop a non-parametric model for a single function  $f(t)$ , imposing  $f(t)$  is orthogonal to a pre-specified set of functions  $g(t) = \{g_1(t), \dots, g_K(t)\}^\top$ , which typically have some physical interpretability. To this end, the authors define orthogonal Gaussian processes through an orthogonal covariance function,  $C_g^\perp(s, t) = C(s, t) - h_g(s)^\top H_g^{-1} h_g(t)$ . The authors show  $f \sim \text{GP}\{0, C_g^\perp(\cdot, \cdot)\}$  is orthogonal to each  $g_1(t), \dots, g_K(t)$  with probability 1. The relationship between NeMO processes and orthogonal Gaussian processes is stated in Proposition 2.5.

**Proposition 2.5.** *Viewing  $\Lambda_{(-k)} = \{\lambda_j\}_{j \neq k}$  as fixed, let  $\lambda_k^\perp \mid \{\lambda_j\}_{j \neq k} \sim \text{GP}\{0, C_{\Lambda_{(-k)}}^\perp\}$  be drawn from a zero-mean Gaussian process orthogonal to  $\Lambda_{(-k)}$ . Also, let  $\{\lambda_1, \dots, \lambda_K\} \sim \mathcal{N}$  with  $\mathcal{N}$  defined in (2). Then,  $\lambda_k \mid \{\lambda_j\}_{j \neq k}$  converges in distribution to  $\lambda_k^\perp \mid \{\lambda_j\}_{j \neq k}$  as  $\nu_\lambda \rightarrow 0$ .*

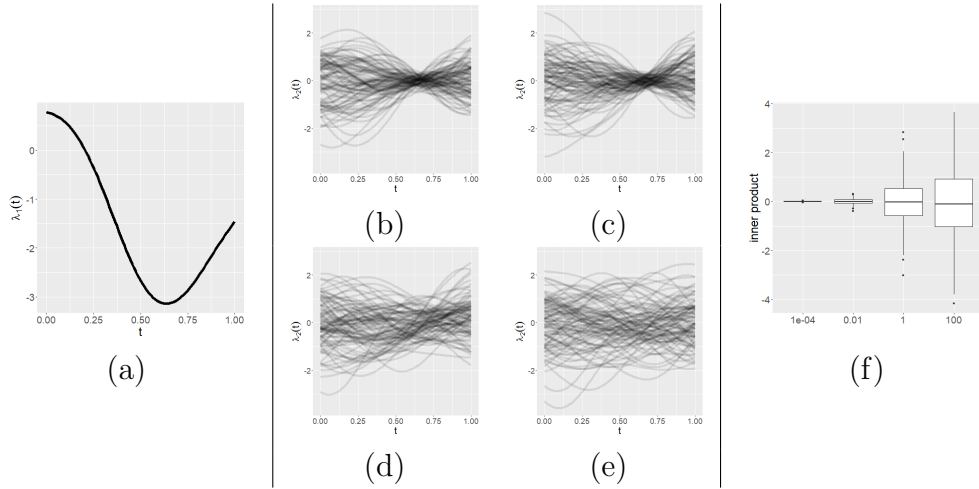


Figure 1: (a) Value of  $\lambda_1$  on which  $\lambda_2$  is conditioned. Realizations of  $\lambda_2 \mid \lambda_1 \sim \text{GP}\{0, C_2^{\nu_\lambda}(\cdot, \cdot)\}$  with  $l_2^2 = .1, \tau_2^2 = 1$  fixed, while (b)  $\nu_\lambda = 0.0001$ , (c)  $\nu_\lambda = 0.01$ , (d)  $\nu_\lambda = 1$ , (e)  $\nu_\lambda = 100$ . (f) Boxplots of 1000 realizations of  $\langle \lambda_1, \lambda_2 \rangle$ , with  $\lambda_2 \mid \lambda_1 \sim \text{GP}\{0, C_2^{\nu_\lambda}(\cdot, \cdot)\}$  with fixed  $l_2^2 = 0.1, \tau_2^2 = 1$  and  $\nu_\lambda = 0.0001, 0.01, 1, 100$ .

While an orthogonal Gaussian process is a prior for a single function orthogonal to a fixed set of functions, NeMO processes provide a prior for a collection of nearly mutually orthogonal functions. Plumlee & Joseph (2018) restrict attention to orthogonal Gaussian processes with continuous sample paths. Proposition 2.6 follows under an analogous assumption that the parent Gaussian processes used to define NeMO processes have continuous sample paths. This verifies the desired property that for any  $j \neq k$  the inner product between  $\lambda_j$  and  $\lambda_k$  converges in probability to zero.

**Proposition 2.6.** *Assuming  $\{\lambda_1, \dots, \lambda_K\} \sim \mathcal{N}$  with  $\mathcal{N}$  defined in (2),  $\langle \lambda_j, \lambda_k \rangle \mid \{\lambda_j\}_{j \neq k}$  converges in probability to 0 for any  $j \neq k$  as  $\nu_\lambda \rightarrow 0$ .*

Proofs for Propositions 2.4, 2.5, and 2.6 are presented in Appendix A.

## 2.3 Role of Covariance Parameters

While the joint distribution defined in Equation (2) is well defined for any choice of covariance kernels  $C_k(\cdot, \cdot)$ ,  $1, \dots, K$ , we illustrate the model based on the squared exponential:

$$C_k(s, t) = \tau_k^2 \exp \left\{ -\frac{1}{2l_k^2}(s - t)^2 \right\}, \quad s, t \in \mathcal{T} \times \mathcal{T}. \quad (5)$$

In a typical Gaussian process, the scale parameters  $\tau_k^2$  determine the spread of realized processes about the mean, while the length-scale parameters  $l_k$  determine the smoothness of realizations.

For a simple setting when  $K = 2$ , we illustrate the conditional prior of Proposition 2.4 when  $\lambda_1$  is sampled from a Gaussian process, shown in panel (a) of Figure 1, and  $C_2$  is defined according to Equation (5). Panels (b)-(e) shows realizations from the prior with  $l_2^2 = .1, \tau_2^2 = 1$  fixed, and  $\nu_\lambda = 0.0001, 0.01, 1, 100$  varying. As discussed in Section 2.2,  $\nu_\lambda$  has an important role in enforcing orthogonality. As  $\nu_\lambda$  increases, the realizations have typical Gaussian process behavior. However, as  $\nu_\lambda$  decreases, the realizations become close to orthogonal to  $\lambda_1$ . When  $\nu_\lambda$  is small, the variance shrinks around  $t \approx .65$ . This is due to the prior's need to offset the extrema of  $\lambda_1$  to enforce orthogonality. Panel (f) shows a boxplot of the inner product between  $\lambda_1$  and 1000 realizations of  $\lambda_2 \mid \lambda_1$  for different values of the penalty parameter  $\nu_\lambda$ . As expected, varying  $\nu_\lambda$  has a drastic effect on the inner product between  $\lambda_1$  and the realizations of  $\lambda_2 \mid \lambda_1$ . The inner product is negligible when  $\nu = 0.0001$  compared to when  $\nu = 100$ .

As discussed in Appendix B, parameters  $l_2^2$  and  $\tau_2^2$  retain their meaning from the typical Gaussian process setting of governing the smoothness and spread of the prior, respectively. Changing  $l_2^2$  and  $\tau_2^2$  with  $\nu_\lambda$  fixed has negligible impact on the inner product between the two functions. In our implementations, we infer  $l_k^2$  and  $\tau_k^2$ , while fixing  $\nu_\lambda$  to be a small value.



# 3 Functional Data Analysis using Nearly Mutually Orthogonal Processes

## 3.1 Observation Model

Letting  $y_i : \mathcal{T} \rightarrow \mathbb{R}$ ,  $i = 1, \dots, n$  denote functional observations, we assume

$$y_i(t) = \mu(t) + \{\lambda_1(t), \dots, \lambda_K(t)\}^\top \eta_i + \epsilon_i(t), \quad i = 1, \dots, n. \quad (6)$$

where  $\mu(t)$  is a mean process common to all observations,  $\lambda_1(t), \dots, \lambda_K(t)$  are functional factor loadings,  $\eta_i \in \mathbb{R}^K$  are latent factors, and  $\epsilon_i(t)$  is a subject-specific error term. Near mutual orthogonality is imposed on  $\lambda_1(t), \dots, \lambda_K(t)$ , and the factors  $\eta_i \in \mathbb{R}^K$  are constrained to have mean close to zero across observations as detailed in Section 3.2.

With sparse and irregular observations, each  $y_i$  is observed on an observation-specific grid  $\vec{t}_i = (t_{i,1}, \dots, t_{i,m_i})^\top$ . Equation (6) can be altered to accommodate this case,

$$y_i(\vec{t}_i) = O_i \mu(t) + O_i \{\lambda_1(\vec{t}_i), \dots, \lambda_K(\vec{t}_i)\}^\top \eta_i + \epsilon_i(\vec{t}_i), \quad i = 1, \dots, n, \quad (7)$$

with  $\vec{t}$  a common grid of size  $m$  merging all observation-specific grid points. Use  $f(\vec{t}) = \{f(t_1), \dots, f(t_m)\}^\top$  to denote a vector of function evaluations. The matrix  $O_i \in \{0, 1\}^{m_i \times m}$  relates the common and observation-specific grids, so that  $O_i f(t) = f(\vec{t}_i)$ . The  $j^{\text{th}}$  row of  $O_i$  is a row vector of 0's with a 1 in the index corresponding to the  $t_{i,j}$  element of  $\vec{t}$ .

We assume independent Gaussian white noise error processes,  $\epsilon_i \sim \text{GP}\{0, C_\epsilon(\cdot, \cdot)\}$ . For  $s, t \in \mathcal{T}$ ,  $C_\epsilon(s, t) = \sigma^2 \delta(s - t)$ , where  $\delta(s - t)$  is the Dirac delta function. For the discretized version of Equation (7), we obtain a Gaussian likelihood,

$$y_i \mid \mu(\vec{t}), \lambda_1(\vec{t}), \dots, \lambda_K(\vec{t}), \eta_i \sim N_{m_i} [O_i \mu(\vec{t}) + O_i \{\lambda_1(\vec{t}), \dots, \lambda_K(\vec{t})\}^\top \eta_i, \sigma^2 I_{m_i}].$$

### 3.2 Prior Specification

We assume a Gaussian process prior for the mean in Equation (6),  $\mu \sim \text{GP}\{0, C_\mu(\cdot, \cdot)\}$ , with  $C_\mu(\cdot, \cdot)$  squared exponential with smoothness  $l_\mu$  and scale  $\tau_\mu^2$ . For the error variance, we assume  $(\sigma^2)^{-1} \sim \text{gamma}(\alpha_\sigma, \beta_\sigma)$ . We further assume  $\{\lambda_1, \dots, \lambda_K\} \sim \mathcal{N}$ . We set  $\nu_\lambda = 1 \times 10^{-4}$  when implementing our model in Sections 4 & 5. We provide a sensitivity analysis of  $\nu_\lambda$  for a simulated dataset in Appendix C. While  $\nu_\lambda$  should be chosen to be small enough so that the loadings are nearly mutually orthogonal, extremely small values can lead to slow Markov chain Monte Carlo mixing. The value  $\nu_\lambda = 1 \times 10^{-4}$  reflects a reasonable balance in our experience.

Latent factors are often constrained to have zero mean (Ramsay & Silverman 2005, Ferraty & Vieu 2006). Let  $\eta_k = (\eta_{1,k}, \dots, \eta_{n,k})^\top$  denote the vector of the  $k^{\text{th}}$  factors for all observations. For equation (6), we impose a relaxed version of the sum-to-zero constraint,  $\sum_{i=1}^n \eta_{i,k} = \eta_k^\top \mathbf{1}_n = 0$ , for  $k = 1, \dots, K$  via a prior that favors  $\eta_k$  values with small sums,

$$\pi(\eta_k) \propto \exp\left(-\frac{1}{2}\eta_k^\top \eta_k\right) \exp\left\{-\frac{1}{2\nu_\eta}(\mathbf{1}_n^\top \eta_k)^2\right\}, \quad (8)$$

independently across  $k$ . The first term in (8) is the kernel of a multivariate Gaussian distribution with identity covariance, while the second term enforces the relaxed sum-to-zero constraint.

Through rearranging the terms in (8), the prior can be recognized as a zero-mean multivariate Gaussian distribution with covariance,

$$\text{var}(\eta_k) = \left(I_n + \frac{1}{\nu_\eta} \mathbf{1}_n \mathbf{1}_n^\top\right)^{-1} = I_n - \frac{1}{\nu_\eta + n} \mathbf{1}_n \mathbf{1}_n^\top.$$

The matrix inversion is computed via Woodbury's formula (Harville 1998). The limiting distribution of  $\eta_k$ , as  $\nu_\eta \rightarrow 0$ , is stated in Proposition 3.1.

**Proposition 3.1.** *Under equation (8),  $\eta_k$  converges in distribution to  $(I_n - \frac{1}{n} \mathbf{1}_n \mathbf{1}_n^\top)N(0, I_n)$*

as  $\nu_\eta \rightarrow 0$ .

Here  $(I_n - \frac{1}{n}1_n1_n^\top)$  is the matrix that projects  $n$ -vectors onto the subspace of vectors that sum to zero. Consequently, when  $\nu_\eta$  is small, the prior enforces a close to sum-to-zero constraint. A proof for this Proposition is presented in Appendix A.

### 3.3 Generalized Functional Factor Analysis

The above methodology can be extended to allow non-Gaussian observations, such as binary or count data. Hall et al. (2008) consider such an extension of the functional data methods in Yao et al. (2005) by using latent Gaussian processes. Bayesian (van der Linde 2009) and frequentist (Goldsmith et al. 2015, Wrobel et al. 2019, Zhong et al. 2021) extensions of James et al. (2000) to allow similar generality have also been proposed.

To modify (6) to allow non-Gaussian  $y_i(t)$ , let

$$\mathbb{E}\{y_i(t) \mid \mu, \lambda_1, \dots, \lambda_K, \eta_i\} = h[\mu(t) + \{\lambda_1(t), \dots, \lambda_K(t)\}^\top \eta_i], \quad i = 1, \dots, n, \quad (9)$$

where  $h(\cdot)$  is a monotone one-to-one and differentiable link function. Model (9) implies the following model for irregular observed data,

$$\mathbb{E}\{y_i(t_i) \mid \mu, \lambda_1, \dots, \lambda_K, \eta_i\} = h[O_i\mu(\vec{t}) + O_i\{\lambda_1(\vec{t}), \dots, \lambda_K(\vec{t})\}^\top \eta_i], \quad i = 1, \dots, n.$$

In the application in Section 5, we consider binary functional data with  $h(\cdot)$  the standard normal cumulative distribution function,  $\Phi$ .

### 3.4 Notes on Computation

We present an adaptive Metropolis-within-Gibbs algorithm to draw  $N$  samples from the joint posterior in Algorithm 1 in Appendix D. Gibbs steps are available for the majority of parameters, and we use adaptive Metropolis steps with proposal variances that are tuned

to meet a target acceptance rate (Andrieu & Thoms 2008, Algorithm 4) for parameters that do not have conditionally conjugate full posterior distributions. In Algorithm 2 of Appendix D, we present an extension of Algorithm 1 for the case of sparse and irregularly sampled binary functional data.

When evaluating the conditional variance  $C_k^{\nu_\lambda}(\cdot, \cdot)$  in Equation (3), we approximate integrals in Equation 4 using Riemann sums. Specifically, we use the approximation  $\int_T f(s)ds \approx \sum_{l=1}^m w_l f(t_l)$  relying on the grid  $\vec{t} = (t_1, \dots, t_m)^\top$ . The weights  $w_l, l = 1, \dots, m$ , are scalars accounting for the spacing of the grid. Letting  $W = \text{diag}(w_1, \dots, w_m)$ , we choose  $w_1 = \frac{t_2 - t_1}{2}$ ,  $w_l = \frac{t_{l+1} - t_{l-1}}{2}$ ,  $l = 2, 3, \dots, m-1$ ,  $w_m = \frac{t_m - t_{m-1}}{2}$ . The approximation error,  $|\int_T f(s)ds - \sum_{l=1}^m w_l f(t_l)|$ , is bounded above by a value proportional to  $\frac{1}{m^2}$ .

The full conditional posterior distribution of  $\lambda_k(\vec{t})$  is given by

$$\begin{aligned} \lambda_k(\vec{t}) | - &\sim N[\mathbb{E}\{\lambda_k(\vec{t}) | -\}, \mathbb{V}\{\lambda_k(\vec{t}) | -\}], \\ \mathbb{V}\{\lambda_k(\vec{t}) | -\} &= \left\{ C_k^{-1}(\vec{t}, \vec{t}) + \frac{1}{\nu_\lambda} W \Lambda_{(-k)}(\vec{t}) \Lambda_{(-k)}(\vec{t})^\top W + \frac{1}{\sigma^2} \sum_{i=1}^n \eta_{i,k}^2 O_i^\top O_i \right\}^{-1} \\ \mathbb{E}\{\lambda_k(\vec{t}) | -\} &= \frac{1}{\sigma^2} \mathbb{V}\{\lambda_k(\vec{t}) | -\} \sum_{i=1}^n \left[ \eta_{i,k} O_i^\top \left\{ y_i(\vec{t}_i) - O_i \mu(\vec{t}) - O_i \sum_{j \neq k} \eta_{i,j} \lambda_j(\vec{t}) \right\} \right]. \end{aligned}$$

Hence, the Gibbs step for the loadings is simple. This step is easily modified to generalized functional factor analysis with binary or categorical observations by using data augmentation (Albert & Chib 1993).

Code to implement functional factor analysis and generalizations on simulated data is available on GitHub: <https://github.com/jamesmatuk/NeMO-FFA>. This repository also contains implementations of all examples presented in this paper. The sign and label ambiguity typical of factor analysis is resolved using Poworoznek et al. (2021).

### 3.5 Selecting the Number of Latent Factors

It is important to have a sensible approach for selecting the dimension of the latent space,  $K$ . We take an over-fitted factor modeling approach with latent space dimension  $K_{\max}$

providing an upper bound on the number of factors. We produce familywise 95% simultaneous credible bands for the factor loadings using the approach in Ruppert et al. (2003). We remove factors having credible intervals containing the zero function, and refit the model. In the examples in this paper, we find that this approach chooses an appropriate number of latent factors, aided by the NeMO prior favoring loadings for unnecessary factors concentrated near zero.

## 4 Simulation Experiments

### 4.1 Functional Factor Analysis for Gaussian Observations

We generate  $n = 100$  functions on a grid,  $\vec{t}$ , with  $m = 30$  equally spaced points, following

$$f_i(\vec{t}) = \mu(\vec{t}) + \{\lambda_1(\vec{t}), \dots, \lambda_K(\vec{t})\}^\top \eta_i, \quad i = 1, \dots, n.$$

With  $K = 2$ , we generate  $\mu$ ,  $\lambda_1$ ,  $\lambda_2$ ,  $\eta_1$ ,  $\eta_2$  according to the priors in Section 3.2 with  $l_\mu^2 = l_{\lambda_1}^2 = l_{\lambda_2}^2 = .4$  and  $\tau_\mu^2 = \tau_{\lambda_1}^2 = \tau_{\lambda_2}^2 = 1$ . Simulated observations are generated according to  $y_i(\vec{t}_i) = f_i(\vec{t}_i) + \epsilon_i(\vec{t}_i)$ , with  $\epsilon_i(\vec{t}_i) \sim N_{m_i}(0, \sigma^2 I_{m_i})$  and  $\sigma^2 = 1$ . The subject specific grids  $\vec{t}_i$  are generated by randomly omitting 25%, 50%, and 75% of the points in the common grid,  $\vec{t}$ . Estimation performance is measured using mean integrated squared error for how well different methods are able to capture  $\mu$ ,  $\lambda_1$ ,  $\lambda_2$ , and all  $f_i$ ,  $i = 1, \dots, n$ .

As competing methods, we use R package `fdapace` to estimate model parameters according to the principal analysis through conditional expectation methodology (Yao et al. 2005). The approach of Yao et al. (2005) uses kernel smoothing to estimate a mean and covariance function from sparse functional data, where individual function estimates rely on these population quantities. Additionally, we use the R package `fpca` to implement the methodology of Peng & Paul (2009). They use a pre-specified basis to represent factor loadings, and inference is carried out through the basis coefficients. The work of Crainiceanu

& Goldsmith (2010) provides an empirical Bayes approach, where the authors mean-center the observations, and estimate a covariance surface using penalized thin-plate splines, from which estimates of factor loadings are computed. While fixing the factor loadings to their estimated values, the authors formulate priors for latent factors and error variance, and perform Markov chain Monte Carlo using **WinBUGS**.

To compare these methods, we replicate data generation 100 times. Figure 2<sup>1</sup> shows mean integrated squared error results for different model parameters and levels of sparsity in panel (a). Boxplots show differences between mean integrated squared error of model parameters between a competing method and our NeMO approach within a simulation replicate. For all methods, estimation performance deteriorates as the sparsity level increases. Consistently, the estimation error from NeMO is lower than the others.

We are also interested in performance in inferring the number of latent factors,  $K = 2$ . We use the approach outlined in Section 3.5 for the NeMO model, while using default choices for competing methods. In Yao et al. (2005) the number of latent factors is set to describe 95% of variability in the observations. In Peng & Paul (2009), the number of factors is selected to minimize a cross validation score. The implementation of Crainiceanu & Goldsmith (2010) assumes the number of factors is given; we provide the method the correct number. Across sparsity levels and replicates, the correct number of factors is chosen 99.7% of the time for NeMO, 2.3% for Yao et al. (2005) and 66% for Peng & Paul (2009).

In Appendix E, we present two additional simulations. In one setting, we simulate data as in this subsection except with lower observation error. In another setting data are generated from a model inferred from the Berkeley growth dataset (Ramsay & Silverman 2005). The assumed generative model coincides with that of Yao et al. (2005). Even in this setting under model misspecification, our functional factor analysis model performs well compared to competitors.

---

<sup>1</sup>Abbreviations in figure legends: CG2010 - Crainiceanu & Goldsmith (2010); PP2009 - Peng & Paul (2009); WZSG2019 - Wrobel et al. (2019); YMW2005 - Yao et al. (2005); ZLLZ2021 - Zhong et al. (2021).

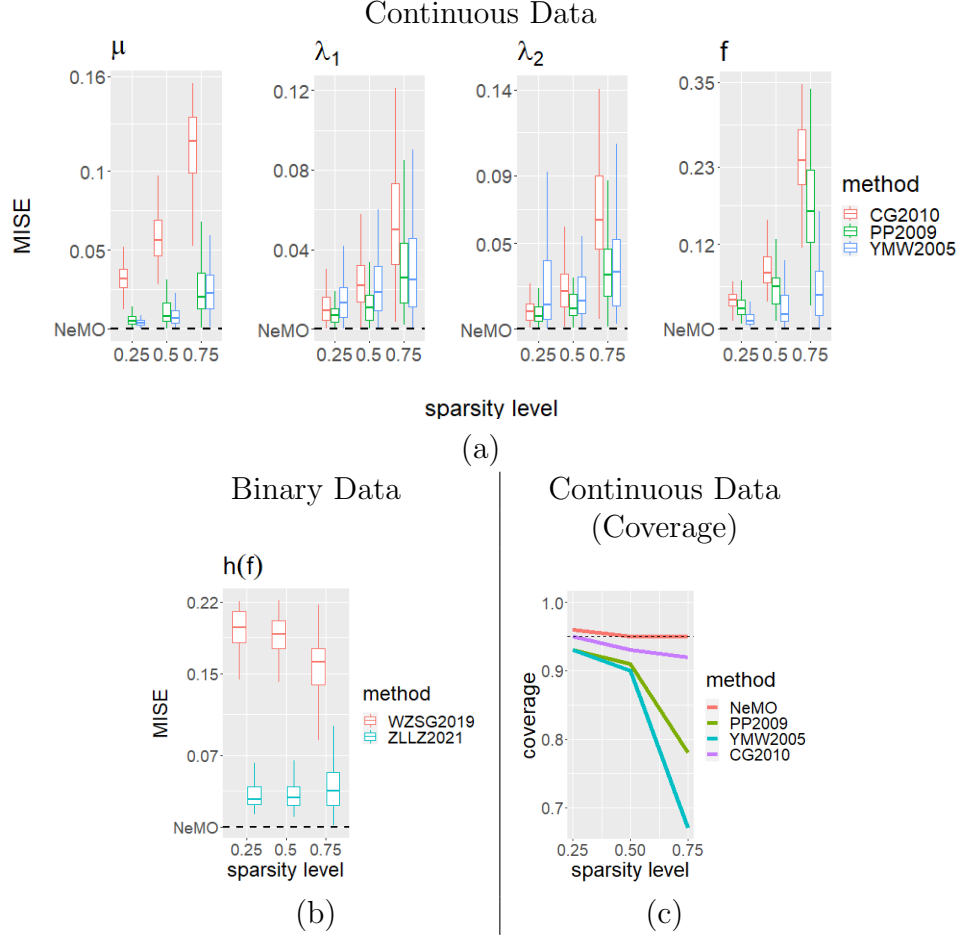


Figure 2: (a) & (b) Mean integrated squared error for estimated parameters at different sparsity levels in the simulations of Sections 4.1 and 4.2, respectively. (c) Coverage of credible/confidence intervals for different methods at different sparsity levels in simulations of Section 4.3.

## 4.2 Estimation for Non-Gaussian Observations

In the generalized functional factor analysis setting, we generate  $n = 100$  binary functions on a grid  $\vec{t}$  with  $m = 30$  equally spaced points according to

$$\text{pr}\{y_i(\vec{t}) = 1\} = h\{f_i(\vec{t})\} = \Phi[\mu(\vec{t}) + \{\lambda_1(\vec{t}), \dots, \lambda_K(\vec{t})\}^\top \eta_i], \quad i = 1, \dots, n,$$

where  $h(\cdot) = \Phi(\cdot)$  is the standard normal cumulative distribution function. With  $K = 2$ , we generate  $\mu$ ,  $\lambda_1$ ,  $\lambda_2$ ,  $\eta_1$ ,  $\eta_2$  according to the priors presented in Section 3.2 with  $l_\mu^2 = l_{\lambda_1}^2 = l_{\lambda_2}^2 = .4$  and  $\tau_\mu^2 = \tau_{\lambda_1}^2 = \tau_{\lambda_2}^2 = 10$ . To study the effect of sparsity, we randomly omit

25%, 50%, and 75% of the observations. Estimation performance of  $h(f_i)$ ,  $i = 1, \dots, n$  is measured through mean integrated squared error.

From our model, we use the posterior mean of  $h[\mu(\vec{t}) + \{\lambda_1(\vec{t}), \dots, \lambda_K(\vec{t})\}^\top \eta_i]$  to produce an estimate of  $h(f_i)$  based on 1,000 Markov chain Monte Carlo iterations. For competitors, we use the `bfpca` function from the `registr` package in R to estimate  $h(f_i)$  using the methodology described in Wrobel et al. (2019). We also estimate  $h(f_i)$  using the methods of Zhong et al. (2021) from the `SLFPCA` R package. Panel (b) of Figure 2 shows the mean integrated squared error results. Each of the boxplots show the difference between the mean integrated squared error of model parameters between a competing method and our NeMO approach within a simulation replicate. Mean integrated squared error from NeMO is consistently below that of the others.

The implementations of Wrobel et al. (2019) and Zhong et al. (2021) do not enable selection of the number of latent factors, so they are fixed to the true number. Using the approach outlined in Section 3.5 for our NeMO model, we select the correct number of latent factors 100% of the time when 25% or 50% of the observations are missing, and 89% of the time when 75% of the data are missing.

In Appendix E, we present an additional simulation, where data are generated as in this subsection, except with a relatively small scale parameter of the factor loadings.

### 4.3 Coverage of Regression Coefficients

We study our model’s ability to serve as the foundation for inferential tasks in a latent factor regression setting (Montagna et al. 2012). Data are generated as in Section 4.1 with  $K = 1$  and  $\eta_{i,1} = \Theta x_{i,1} + \xi_{i,1}$ , where  $x_{i,1}$  is an observed covariate,  $\Theta$  is a regression coefficient and  $\xi_{i,1} \sim N(0, 1)$  are independent. In each of 100 replicates,  $\Theta$  and  $x_{i,1}$  are independently generated as standard normal random variables. We study frequentist coverage of 95% credible intervals for  $\Theta$  based on 10,000 Markov chain Monte Carlo samples. For comparison, we estimate  $\eta_{i,1}$ ,  $i = 1, \dots, n$ , using the methods of Yao et al. (2005) and



Peng & Paul (2009) from Section 4.1 and regress the estimated factors onto the covariate. For the method of Crainiceanu & Goldsmith (2010), the latent factor regression is a hierarchical layer in the model. Figure 2 panel (c) show interval coverage when  $\sigma^2 = 1$ . These results illustrate the importance of uncertainty propagation between estimation and inference. The coverage for Peng & Paul (2009) and Yao et al. (2005) is very low due to conditioning on first stage estimates. The low coverage of Crainiceanu & Goldsmith (2010) is due to the empirical Bayes setup, which fails to account for uncertainty in estimating factor loadings. In either setting NeMO propagates uncertainty between estimation and inference improving performance.

In Appendix E, we present an additional simulation, where data are simulated as in this subsection except with a relatively small error variance.

## 5 Cebu Longitudinal Health and Nutrition Survey

The Cebu Longitudinal Health and Nutrition Survey is an ongoing multi-generational study (Adair et al. 2011). The focus is on maternal, child, and environmental factors and their connection to health, social, and economic outcomes for mother-child pairs in the metropolitan area of Cebu, Philippines. Refer to <https://cebu.cpc.unc.edu/>. The weight of the infants and other covariates were recorded in 2 month intervals from birth to 2 years of age. Previous work (Adair et al. 1993, Adair & Guilkey 1997) found that scalar covariates, such as height of the mother, sex of the child, area (urban or rural) where the family lives, season of birth (rainy or dry), and longitudinal covariates, such as breastfeeding status and illness, are associated with weight dynamics in early childhood.

We implement the following flexible model for the weight dynamics,

$$\begin{aligned}
y_i(\vec{t}_i) &= O_i\mu(\vec{t}) + O_i\{\lambda_1(\vec{t}), \dots, \lambda_K(\vec{t})\}^\top \eta_i + O_i \sum_{j=1}^4 \int_T \beta_j(s, \vec{t}) z_{i,j}(s) ds + \epsilon_i(\vec{t}_i) \\
\eta_i &= \Theta x_i + \xi_i
\end{aligned}$$

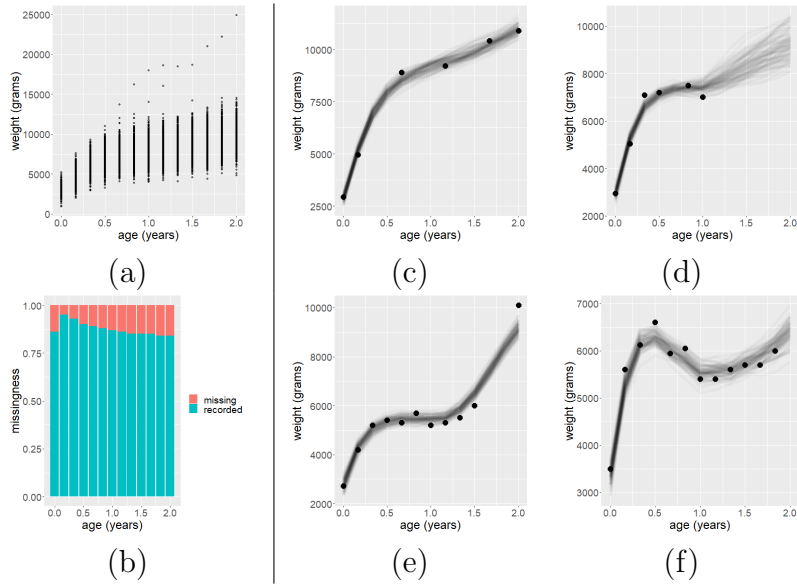


Figure 3: (a) Weight by age for  $n = 2898$  children in the Cebu Longitudinal Health and Nutrition Survey. (b) Proportion of missing weight data by age. (c)-(f) Posterior samples of fitted weight trajectories,  $\mu(\vec{t}) + \{\lambda_1(\vec{t}), \dots, \lambda_5(\vec{t})\}^\top \eta_i + \sum_{j=1}^4 \int_T \beta_j(s, \vec{t}) z_{i,j}(s) ds$  overlaid on  $y_i(\vec{t}_i)$  for  $i = 421, 1626, 2601$ .

The longitudinal recordings of weight of the  $i^{\text{th}}$  child are denoted by  $y_i(\vec{t}_i)$ , where the observation-specific grid points  $\vec{t}_i$  are a subset of  $\vec{t} = (0, \frac{1}{2}, \dots, \frac{24}{2})^\top$ , representing the two month intervals on which the measurements are recorded. We use the functional factor analysis approach developed in Section 3 for  $\mu, \lambda_1, \dots, \lambda_K$  and  $\xi_i$ .

The response can vary with the scalar covariates,  $x_i \in \mathbb{R}^4$ , mentioned above through a latent factor regression setup (Montagna et al. 2012). The coefficient matrix  $\Theta \in \mathbb{R}^{K \times 4}$  models the relationship between the latent factors and the scalar covariates. To account for longitudinal covariates,  $z_{i,j}(s)$ ,  $j = 1, \dots, 4$ , we use a functional linear model (Ramsay & Dalzell 1991). These covariates are sparsely recorded and track if a child is fed breast milk and 3 indicators of illness (diarrhea, fever, and cough). We use our generalized functional factor analysis approach for model-based imputation of these covariates for the functional linear model to be well defined. For the coefficient surface  $\beta_1(s, t)$  corresponding to the breast milk indicator, we specify  $\beta_1(s, t) = 0$  for  $s > t$  in a historical linear model approach (Malfait & Ramsay 2003). Through this setup, weight at time  $t$  is only affected by breastfeeding status at earlier ages. For the coefficient surface of the three illness indicators

$\beta_2(s, t)$ ,  $\beta_3(s, t)$ ,  $\beta_4(s, t)$ , we specify  $\beta_j(s, t) = 0$  for  $s \neq t$ ,  $j = 2, 3, 4$  in a concurrent linear model (Hastie & Tibshirani 1993). Through this setup the illness status of a child at time  $t$  only effects the weight at time  $t$ . Full details of the hierarchical model specification are presented in Appendix F.

We base inference on  $n = 2898$  mother-child pairs of the 3327 pairs originally enrolled in the study. We excluded subjects due to child death, the family moving out of the Cebu metropolitan area, refusal to participate after the baseline survey, or if there was no covariate or response data recorded. In the remaining  $n = 2898$  subjects, sparsity in the response and longitudinal covariates tends to arise due to a missed survey or failure to answer a specific question. Posterior inference is based on 100,000 Markov chain Monte Carlo samples (to be conservative), where convergence is assessed using trace plot diagnostics, shown in Appendix F.

Figure 3 panel (a) displays the weight of all children measured every two months from birth to age 2 and panel (b) displays the proportion of missing observations by age. In panels (c)-(f), we plot weight measurements,  $y_i(\vec{t}_i)$ , for a few children along with posterior samples of  $\mu(\vec{t}) + \{\lambda_1(\vec{t}), \dots, \lambda_5(\vec{t})\}^\top \eta_i + \sum_{j=1}^4 \int_T \beta_j(s, \vec{t}) z_{i,j}(s) ds$ . The model is able to fit a variety of shapes of underlying functions, with greater uncertainty at ages where the child’s weight was not observed, such as panel (d). The functional factor loadings,  $\lambda_1, \dots, \lambda_K$ , are able to describe modes of variability in weight dynamics. We implement our approach described in Section 3.5 to select the number of latent factors. Starting with an over-fitted factor model, our approach automatically forces the loadings for extra unnecessary factors to be close to zero. We provide an illustration in Appendix F.

The effect of the scalar covariates on the response is modeled through the latent factors,  $\eta_i = \Theta x_i + \xi_i$ . With all other variables held constant, the effect of a unit increase of a single covariate on the response is given by  $\{\lambda_1(\vec{t}), \dots, \lambda_5(\vec{t})\}^\top \Theta_q$ , where  $\Theta_q$  denotes the  $q^{\text{th}}$  column of the matrix  $\Theta$ , for  $q = 1, \dots, 4$ . Posterior samples of these functions are shown in Figure 4. Panel (a) shows the inferred effect of a unit increase in mother’s height on child weight. The model infers that children with taller mothers generally weigh more.

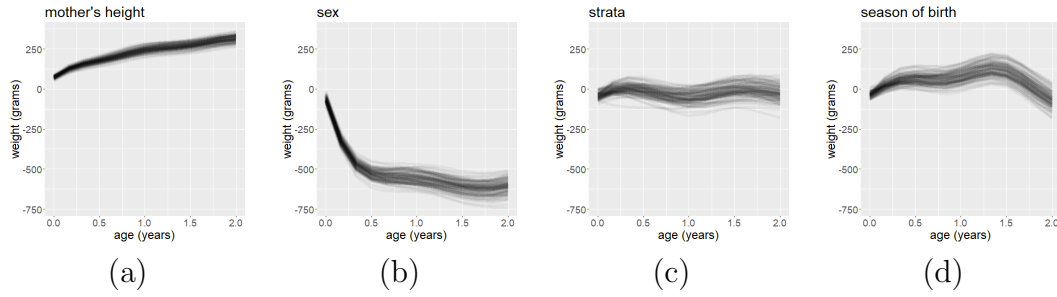


Figure 4: (a)-(d) Posterior samples of  $(\lambda_1(\vec{t}), \dots, \lambda_5(\vec{t}))^\top \Theta_q$  for  $q = 1, \dots, 4$ , representing the effect of the scalar covariates (height of the mother, sex of the child, area (urban or rural) where the family lives, season of birth (rainy or dry)) on weight. Mother's height and sex of child are clearly associated with weight dynamics. Strata and season of birth appear to have near zero effects with relatively high uncertainty.

Panel (b) shows the inferred difference in weight between male and female children, where  $x_{i,2} = 0$  if the  $i^{\text{th}}$  subject is male. The model infers that female children generally weigh less than male children. The discrepancy in weight is small at birth, but changes rapidly from birth to 6 months. Panel (c) shows the inferred difference between children born in urban or rural strata, where  $x_{i,3} = 0$  if the  $i^{\text{th}}$  subject was born in an urban area. Panel (d) shows the inferred difference between children born in the rainy or dry season, where  $x_{i,4} = 0$  if the  $i^{\text{th}}$  subject was born during the rainy season. Compared to mother's height or sex, these covariate effects are smaller in magnitude with greater uncertainty.

In order to compute the integral  $\int_T \beta_1(s, \vec{t}) z_{i,1}(s) ds$  related to the functional linear model relating breastfeeding status to weight, we rely on generalized functional factor analysis for model based imputation of the binary functional data  $z_{i,1}$ ,  $i = 1, \dots, n$ . Specifics of the model based imputation and posterior visualization are given in Appendix F. Generalized functional factor loadings capture if a child was breastfed at all and when breastfeeding was discontinued.

In order to understand the effects of breastfeeding on child weight, we study posterior samples of the functions  $\int_T \beta_1(s, s') 1_{s \leq s'} ds$ , where  $1_{s \leq s'}$  denotes the indicator function. These functions capture the effect of breastfeeding on weight at  $s'$  years with other variables held constant. They can be compared to the effect of never breastfeeding captured by the zero function. Figure 5 shows the effect of breastfeeding for  $s' = 0, 0.5, 1, 2$  years. If a child

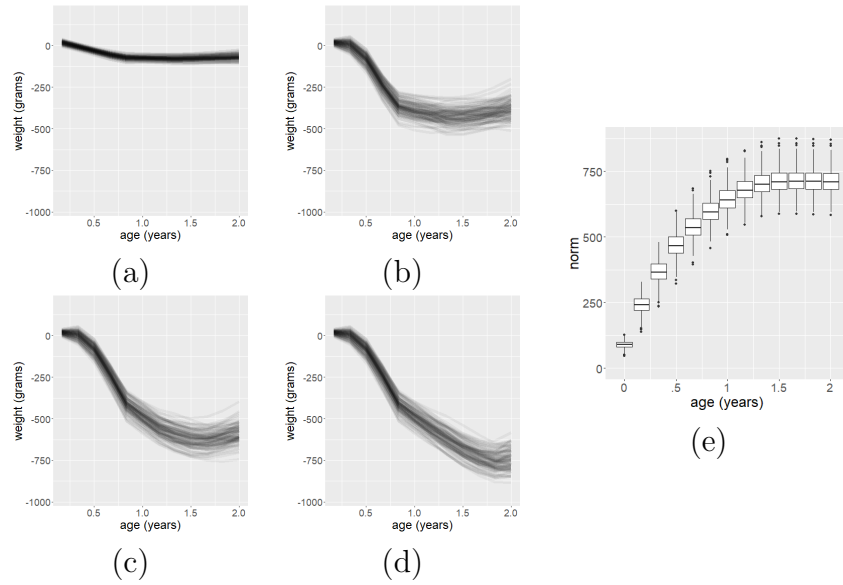


Figure 5: (a)-(d) Posterior samples of  $\int_{\mathcal{T}} \beta_1 1_{s \leq s'} ds$  for  $s' = 0, 0.5, 1, 2$  years, representing the effect of breastfeeding for different durations on weight. (e) Boxplots of posterior samples of  $\|\int_{\mathcal{T}} \beta_1 1_{s \leq s'} ds\|_2$  for different values of  $s'$ , representing the magnitude of the effect of breastfeeding for different durations. Children that are fed breast milk tend to weigh less than non-breast milk fed counterparts. The effect of breastfeeding on weight dynamics tends to level off after 1 year.

is breastfed only at birth, the effect is close to a zero (panel (a)). While breastfed and non-breastfed children are similar in weight at a younger age, their discrepancy is pronounced at larger ages, where breastfed children tend to weigh less. This difference is exaggerated the longer that a child is breastfed (panels (b) through (d)). The effect of breastfeeding tends to level off, as shown through  $\|\int_{\mathcal{T}} \beta_1(s, s') 1_{s \leq s'} ds\|_2$  for different values of  $s'$  shown in panel (e). Continuing breastfeeding for more months in the first year has a significant impact on weight, while continuing longer after age 1 has a relatively small impact. These inferences corroborate past work devoted to studying the effects of breastfeeding. Dewey (1998) conduct a meta-analysis studying effects of breastfeeding on child growth outcomes, including weight, height and head circumference. They report that breastfed infants tend to self-regulate food intake, have lower observable metabolic rates, and are leaner than their non-breastfed counterparts. The differences in weight between breastfed and non-breastfed children tend to be noticeable after 6 months of age.

For the illness longitudinal covariates we assume a concurrent regression model, which simplifies the integrals,  $\int_T \beta_j(s, t) z_{i,j}(s) ds = \beta_j(t) z_{i,j}(t)$ , for all  $j = 2, 3, 4$ ,  $i = 1 \dots, n$ . Similar to the breastfeeding functions, the illness indicators are sparsely recorded so we rely on model based imputation from our generalized functional factor analysis model. In terms of the effect on weight of experiencing an illness, Diarrhea tends to affect weight more than fever, and fever tends to affect weight more than cough. These regression functions tend to be more negative at higher ages. We speculate that the effects of diarrhea and fever affect weight more than cough because they can lead to dehydration (National Library of Medicine (US) 2022). We provide modeling details and posterior visualization in Appendix F.

In Appendix F, we present an analysis of these data using Crainiceanu & Goldsmith (2010). The inferential results are generally consistent with our NeMO-based analysis with a few marked differences. In the competing model, there is no ability to propagate uncertainty in the estimated mean process and factor loadings while inferring covariate effects on weight. Consequently, the empirical Bayes setup of the competing model can distort the inferences made about effect sizes. There are discrepancies between the competing model and the NeMO model in the magnitude of effects of season of birth and breastfeeding. In the competing model, season of birth has a larger effect on weight, and breastfeeding has a smaller effect on weight. To further compare the two models, we use the widely applicable information criterion to assess predictive performance (Vehtari et al. 2017), with preference for the NeMO model (69709.10) compared to the model of Crainiceanu & Goldsmith (2010) (69905.07).

In Appendix F, we assess fit of the NeMO model by residual analysis, performing posterior predictive checks and considering reduced models omitting covariates with seemingly small effects. We find that the model is adequate in describing individual and population level features of the observations, and the full model with all covariates considered is preferred over reduced models according to the widely applicable information criterion. For this dataset, we conclude that the model provides reasonable fit to the observations while

enabling interpretable inference with uncertainty quantification.

## 6 Discussion

There is a rich literature on Bayesian factor analysis, and the problem of how to best choose a prior for high-dimensional loadings vectors that also allows for uncertainty in the number of factors. It is particularly popular to take an over-fitted factor modeling approach, starting with an upper bound on the number of factors  $K$  and then choosing a shrinkage prior that favors setting columns of the loadings matrix for unnecessary factors equal to zero (Bhattacharya & Dunson 2011, Schiavon et al. 2022). In this article we also take an over-fitted factor modeling approach, but instead of shrinking loadings towards zero, we shrink strongly towards orthogonality to avoid the factor splitting problem and automatically force redundant factors to have loadings close to zero. In future work, it will be interesting to further study this approach including outside of the functional data setting.

One aspect of functional data that we have not considered is phase variability, corresponding to the variability of the relative timing of functional features, such as extrema. Marron et al. (2015) discuss this concept and state that models that explicitly account for this variability can be more parsimonious. In future work, we plan to extend our model to account for phase variability, along the lines of Kneip & Ramsay (2008), Earls & Hooker (2017). One challenge is developing a prior model for phase that is computationally efficient and can scale to large samples.

Although we have focused on a version of nearly mutually orthogonal processes, which starts with independent parent Gaussian processes, the same type of approach can be applied using alternative parent processes. For example, it is automatic to consider multivariate Gaussian parent distributions, obtaining new types of methods for Bayesian factor analysis. It is also interesting to consider more intricate parent processes, such as Lévy processes.

## Acknowledgements

This work was supported by NIH grants RO1ES027489 and R01ES028804.



# Supplemental Material: Bayesian modeling of nearly mutually orthogonal processes

## Abstract

This is the supplemental material for the paper entitled ‘Bayesian modeling of nearly mutually orthogonal processes’. In Section A, we present proofs for the propositions stated in the main paper. In Section B, we present figures that illustrate the role of covariance hyperparameters in the prior. In Section C, we study the sensitivity of the posterior to  $\nu_\lambda$  for a simulated dataset. In Section D, we provide full implementation details for the functional factor analysis models and generalized functional factor analysis model for binary functional data. In Section E, we present an additional simulation examples. In Section F, we provide additional details related to the data analysis of the Cebu Longitudinal Health and Nutritional Survey.

## A Proofs

**Proposition A.1.** *Let  $E := \{\lambda_1, \dots, \lambda_K \in \mathcal{H} \mid \langle \lambda_j, \lambda_k \rangle \neq 0, \text{ for some } j \neq k\}$ . For any measurable subset  $E' \subseteq E$ ,  $\lim_{\nu_\lambda \rightarrow 0} \mathcal{N}(E') = 0$ .*

*Proof.* For any  $(\lambda_1, \dots, \lambda_K) \in E'$ ,  $\lim_{\nu_\lambda \rightarrow 0} \exp \left\{ -\frac{1}{2\nu_\lambda} \sum_{k=1}^K \sum_{j < k} \langle \lambda_j, \lambda_k \rangle^2 \right\} = 0$ .

By definition of  $\mathcal{N}$ ,

$$\lim_{\nu_\lambda \rightarrow 0} \mathcal{N}(E') \propto \lim_{\nu_\lambda \rightarrow 0} \int_{E'} \exp \left\{ -\frac{1}{2\nu_\lambda} \sum_{k=1}^K \sum_{j < k} \langle \lambda_j, \lambda_k \rangle^2 \right\} d\mathcal{G}(\lambda_1, \dots, \lambda_K) \quad (10)$$

$$\begin{aligned} &= \int_{\mathcal{H}} \lim_{\nu_\lambda \rightarrow 0} 1_{\{\lambda_1, \dots, \lambda_K \in E'\}} \exp \left\{ -\frac{1}{2\nu_\lambda} \sum_{k=1}^K \sum_{j < k} \langle \lambda_j, \lambda_k \rangle^2 \right\} d\mathcal{G}(\lambda_1, \dots, \lambda_K) \quad (11) \\ &= \int_{\mathcal{H}} 0 d\mathcal{G}(\lambda_1, \dots, \lambda_K) = 0. \end{aligned}$$

The equality from Equation (10) to (11) follows from the Bounded Convergence Theorem,

since  $\exp \left\{ -\frac{1}{2\nu_\lambda} \sum_{k=1}^K \sum_{j < k} \langle \lambda_j, \lambda_k \rangle^2 \right\} \leq 1$ .

□

**Proposition A.2.** For any measurable set  $A \subseteq \mathcal{H}$ ,  $\lim_{\nu_\lambda \rightarrow \infty} \mathcal{N}(A) = \mathcal{G}(A)$ .

*Proof.* For any measurable subset  $A \subset \mathcal{H}$ ,  $\lim_{\nu_\lambda \rightarrow \infty} \exp \left\{ -\frac{1}{2\nu_\lambda} \sum_{k=1}^K \sum_{j < k} \langle \lambda_j, \lambda_k \rangle^2 \right\} = 1$  for any  $\lambda_1, \dots, \lambda_K \in A$ .

By definition of  $\mathcal{N}$ ,

$$\lim_{\nu_\lambda \rightarrow \infty} \mathcal{N}(A) \propto \lim_{\nu_\lambda \rightarrow \infty} \int_A \exp \left\{ -\frac{1}{2\nu_\lambda} \sum_{k=1}^K \sum_{j < k} \langle \lambda_j, \lambda_k \rangle^2 \right\} d\mathcal{G}(\lambda_1, \dots, \lambda_K) \quad (12)$$

$$= \int_{\mathcal{H}} \lim_{\nu_\lambda \rightarrow \infty} 1_{\{\lambda_1, \dots, \lambda_K \in A\}} \exp \left\{ -\frac{1}{2\nu_\lambda} \sum_{k=1}^K \sum_{j < k} \langle \lambda_j, \lambda_k \rangle^2 \right\} d\mathcal{G}(\lambda_1, \dots, \lambda_K) \quad (13)$$

$$= \int_{\mathcal{H}} 1_{\{\lambda_1, \dots, \lambda_K \in A\}} d\mathcal{G}(\lambda_1, \dots, \lambda_K) = \int_A d\mathcal{G}(\lambda_1, \dots, \lambda_K) = \mathcal{G}(A).$$

The equality from Equation (12) to (13) follows from the Bounded Convergence Theorem, since  $\exp \left\{ -\frac{1}{2\nu_\lambda} \sum_{k=1}^K \sum_{j < k} \langle \lambda_j, \lambda_k \rangle^2 \right\} \leq 1$ . Note that in Equation (12), the constant of proportionality is  $\left( \lim_{\nu_\lambda \rightarrow \infty} \int_{\mathcal{H}} \exp \left\{ -\frac{1}{2\nu_\lambda} \sum_{k=1}^K \sum_{j < k} \langle \lambda_j, \lambda_k \rangle^2 \right\} d\mathcal{G}(\lambda_1, \dots, \lambda_K) \right)^{-1} = \mathcal{G}(\mathcal{H})^{-1} = 1$ .  $\square$

**Proposition A.3.** Let  $E_\omega := \{\lambda_1, \dots, \lambda_K \in \mathcal{H} \mid \sum_{k=1}^K \sum_{j < k} \langle \lambda_j, \lambda_k \rangle^2 > \omega\}$ . For any  $\nu_\lambda > 0$  and measurable subset  $E'_\omega \subseteq E_\omega$  with non-zero  $\mathcal{G}(E'_\omega)$ ,

$$\frac{\mathcal{N}(E'_\omega)}{\mathcal{G}(E'_\omega)} \leq F \exp \left( -\frac{\omega}{2\nu_\lambda} \right),$$

where  $F = \left( \mathbb{E}_{\mathcal{G}} \left[ \exp \left\{ -\frac{1}{2\nu_\lambda} \sum_{k=1}^K \sum_{j < k} \langle \lambda_j, \lambda_k \rangle^2 \right\} \right] \right)^{-1}$  is a normalizing constant.

*Proof.* Note that for any  $\lambda_1, \dots, \lambda_K \in E'_\omega$ ,  $\exp \left\{ -\frac{1}{2\nu_\lambda} \sum_{k=1}^K \sum_{j < k} \langle \lambda_j, \lambda_k \rangle^2 \right\} \leq \exp \left( -\frac{\omega}{2\nu_\lambda} \right)$ .

By the definition of  $\mathcal{N}$ ,

$$\begin{aligned}
\mathcal{N}(E'_\omega) &= F \int_{E'_\omega} \exp \left\{ -\frac{1}{2\nu_\lambda} \sum_{k=1}^K \sum_{j < k} \langle \lambda_j, \lambda_k \rangle^2 \right\} d\mathcal{G}(\lambda_1, \dots, \lambda_K) \\
&= F \int_{\mathcal{H}} 1_{\{\lambda_1, \dots, \lambda_K \in E'_\omega\}} \exp \left\{ -\frac{1}{2\nu_\lambda} \sum_{k=1}^K \sum_{j < k} \langle \lambda_j, \lambda_k \rangle^2 \right\} d\mathcal{G}(\lambda_1, \dots, \lambda_K) \\
&\leq F \exp \left( -\frac{\omega}{2\nu_\lambda} \right) \int_{E'_\omega} d\mathcal{G}(\lambda_1, \dots, \lambda_K) = F \exp \left( -\frac{\omega}{2\nu_\lambda} \right) \mathcal{G}(E'_\omega)
\end{aligned}$$

Since we assumed  $\mathcal{G}(E'_\omega) > 0$ , it follows

$$\frac{\mathcal{N}(E'_\omega)}{\mathcal{G}(E'_\omega)} \leq F \exp \left( -\frac{\omega}{2\nu_\lambda} \right).$$

□

**Proposition A.4.** *Given  $\{\lambda_j\}_{j \neq k}$ ,  $\lambda_k$  is a zero-mean Gaussian process with covariance*

$$C_k^{\nu_\lambda}(s, t) = C_k(s, t) - h_{\Lambda_{(-k)}}(s)^\top \{\nu_\lambda I_{K-1} + H_{\Lambda_{(-k)}}\}^{-1} h_{\Lambda_{(-k)}}(t), \text{ where} \quad (14)$$

$$h_{\Lambda_{(-k)}}(t) = \int_{\mathcal{T}} C_k(s, t) \Lambda_{(-k)}(s) ds, \quad H_{\Lambda_{(-k)}} = \int_{\mathcal{T}} \int_{\mathcal{T}} C_k(s, s') \Lambda_{(-k)}(s) \Lambda_{(-k)}(s')^\top ds ds' \quad (15)$$

with  $\Lambda_{(-k)}(s) = \{\lambda_1(s), \dots, \lambda_{k-1}(s), \lambda_{k+1}(s), \dots, \lambda_K(s)\}^\top$ .

*Proof.* Let  $H_k$  denote the reproducing kernel Hilbert space defined by the  $k^{\text{th}}$  parent Gaussian process, with Gaussian measure  $\mathcal{G}_k$ . Similarly, let  $H_{(-k)}$  denote the product reproducing kernel Hilbert spaces defined by all parent Gaussian Processes except the  $k^{\text{th}}$ , with

Gaussian product measure  $\mathcal{G}_{(-k)}$ . Then, for any measurable  $A \subset H_k$  and  $B \subset H_{(-k)}$ ,

$$\begin{aligned}
P_{\mathcal{N}}(\lambda_k \in A, \{\lambda_j\}_{j \neq k} \in B) &\propto \\
&\int_{\mathcal{H}} 1_{\{\lambda_k \in A, \{\lambda_j\}_{j \neq k} \in B\}} \exp \left\{ -\frac{1}{2\nu_\lambda} \sum_{k=1}^K \sum_{j < k} \langle \lambda_j, \lambda_k \rangle^2 \right\} d\mathcal{G}(\lambda_1, \dots, \lambda_K) \\
&= \int_{\mathcal{H}_{(-k)}} \int_{\mathcal{H}_k} 1_{\{\lambda_k \in A\}} \exp \left\{ -\frac{1}{2\nu_\lambda} \sum_{j \neq k} \langle \lambda_j, \lambda_k \rangle^2 \right\} d\mathcal{G}_k(\lambda_k) \\
&\quad \times 1_{\{\{\lambda_j\}_{j \neq k} \in B\}} \exp \left\{ -\frac{1}{2\nu_\lambda} \sum_{j \neq k} \sum_{j' < j} \langle \lambda_j, \lambda_{j'} \rangle^2 \right\} d\mathcal{G}_{(-k)}(\{\lambda_j\}_{j \neq k}), \\
&= \int_B \int_A \exp \left\{ -\frac{1}{2\nu_\lambda} \sum_{j \neq k} \langle \lambda_j, \lambda_k \rangle^2 \right\} d\mathcal{G}_k(\lambda_k) d\mathcal{N}_{(-k)}(\{\lambda_j\}_{j \neq k}),
\end{aligned}$$

where  $\mathcal{N}_{(-k)}$  is the NeMO measure defined using all parent Gaussian processes except the  $k^{\text{th}}$ . We denote  $\mathcal{N}_k(A) \propto \int_A \exp \left\{ -\frac{1}{2\nu_\lambda} \sum_{j \neq k} \langle \lambda_j, \lambda_k \rangle^2 \right\} d\mathcal{G}_k(\lambda_k)$ , which is the conditional probability measure (Resnick 2019, Section 5.8) induced by  $\lambda_k \mid \{\lambda_j\}_{j \neq k}$ , when  $\lambda_1, \dots, \lambda_K \sim \mathcal{N}$ .

To show  $\lambda_k \mid \{\lambda_j\}_{j \neq k}$  is a Gaussian process, we will show the conditional characteristic functional  $\mathbb{E}_{\mathcal{N}_k}[\exp \{i\langle U, \lambda_k \rangle\} \mid \{\lambda_j\}_{j \neq k}]$  coincides with the characteristic functional of a zero-mean Gaussian process with covariance function  $C_k^{\nu_\lambda}(\cdot, \cdot)$ , for any function  $U \in \mathcal{H}_k$  that satisfies  $\mathbb{E}_{\mathcal{N}_k}[\exp \{i\langle U, \lambda_k \rangle\} \mid \{\lambda_j\}_{j \neq k}] < \infty$ . We will make use of the lower Riemann sum, which satisfies  $\frac{\lfloor T \rfloor}{m} \sum_{l=1}^m U(t_l^*) \lambda_k(t_l^*) \leq \langle U, \lambda_k \rangle$  for  $t_l = a + l \frac{(b-a)}{m}$ ,  $l = 0, 1, \dots, m$ ,  $t_l^* \in [t_{l-1}, t_l]$ ,  $l = 1, \dots, m$ ,  $T = [a, b]$ . In general, we use  $f(\vec{t}^*) = (f(t_1^*), \dots, f(t_m^*))^\top$  to denote a vector of function evaluations on the grid  $\vec{t}^* = (t_1^*, \dots, t_m^*)^\top$ .

First, note

$$\begin{aligned}
& \mathbb{E}_{\mathcal{G}_k} \left[ \exp \left\{ -\frac{1}{2\nu_\lambda} \sum_{j \neq k} \langle \lambda_j, \lambda_k \rangle^2 \right\} \mid \{ \lambda_j \}_{j \neq k} \right] \\
&= \mathbb{E}_{\mathcal{G}_k} \left[ \lim_{m \rightarrow \infty} \exp \left\{ -\frac{|T|^2}{2\nu_\lambda m^2} \lambda_j(\vec{t}^*)^\top \Lambda_{-k}(\vec{t}^*) \Lambda_{-k}(\vec{t}^*)^\top \lambda_j(\vec{t}^*) \right\} \mid \{ \lambda_j \}_{j \neq k} \right] \\
& \tag{16}
\end{aligned}$$

$$\begin{aligned}
&= \lim_{m \rightarrow \infty} \int_{\mathbb{R}^m} \exp \left\{ -\frac{|T|^2}{2\nu_\lambda m^2} \lambda_j(\vec{t}^*)^\top \Lambda_{-k}(\vec{t}^*) \Lambda_{-k}(\vec{t}^*)^\top \lambda_j(\vec{t}^*) \right\} \\
&\times (2\pi \det [C_k(\vec{t}^*, \vec{t}^*)])^{-\frac{1}{2}} \exp \left\{ -\frac{1}{2} \lambda_j(\vec{t}^*)^\top C_k(\vec{t}^*, \vec{t}^*)^{-1} \lambda_j(\vec{t}^*) \right\} d\lambda_k(\vec{t}^*) \\
& \tag{17}
\end{aligned}$$

$$= \det [C_k(\vec{t}^*, \vec{t}^*)]^{-\frac{1}{2}} \det \left[ C_k(\vec{t}^*, \vec{t}^*)^{-1} + \frac{|T|^2}{\nu_\lambda m^2} \Lambda_{-k}(\vec{t}^*) \Lambda_{-k}(\vec{t}^*)^\top \right]^{-\frac{1}{2}}$$

where the interchange of expectation and the limit from Equation (16) to (17) follows from the bounded convergence theorem, since  $\exp \left\{ -\frac{|T|^2}{2\nu_\lambda m^2} \lambda_j(\vec{t}^*)^\top \Lambda_{-k}(\vec{t}^*) \Lambda_{-k}(\vec{t}^*)^\top \lambda_j(\vec{t}^*) \right\} \leq 1$ .

Similarly, note

$$\begin{aligned}
& \mathbb{E}_{\mathcal{G}_k} \left[ \exp \{ i \langle U, \lambda_k \rangle \} \exp \left\{ -\frac{1}{2\nu_\lambda} \sum_{j \neq k} \langle \lambda_j, \lambda_k \rangle^2 \right\} \mid \{ \lambda_j \}_{j \neq k} \right] \\
&= \lim_{m \rightarrow \infty} \int_{\mathbb{R}^m} \exp \left\{ i \frac{|T|}{m} U(\vec{t}^*)^\top \lambda_k(\vec{t}^*) \right\} (2\pi \det [C_k(\vec{t}^*, \vec{t}^*)])^{-\frac{1}{2}} \\
&\times \exp \left\{ -\frac{1}{2} \lambda_j(\vec{t}^*)^\top (C_k(\vec{t}^*, \vec{t}^*)^{-1} + \frac{|T|^2}{\nu_\lambda m^2} \Lambda_{-k}(\vec{t}^*) \Lambda_{-k}(\vec{t}^*)^\top) \lambda_j(\vec{t}^*) \right\} d\lambda_k(\vec{t}^*), \\
& \tag{18}
\end{aligned}$$

where the interchange of expectation and limit in Equation (18) follows from the bounded convergence theorem, since  $\left| \exp \left\{ i \frac{|T|}{m} U(\vec{t}^*)^\top \lambda_k(\vec{t}^*) - \frac{|T|^2}{2\nu_\lambda m^2} \lambda_j(\vec{t}^*)^\top \Lambda_{-k}(\vec{t}^*) \Lambda_{-k}(\vec{t}^*)^\top \lambda_j(\vec{t}^*) \right\} \right| \leq 1$ .

Finally, consider

$$\begin{aligned}
\mathbb{E}_{\mathcal{N}_k}[\exp\{i\langle U, \lambda_k \rangle\} \mid \{\lambda_j\}_{j \neq k}] &= \frac{\mathbb{E}_{\mathcal{G}_k}[\exp\{i\langle U, \lambda_k \rangle\} \exp\{-\frac{1}{2\nu_\lambda} \sum_{j \neq k} \langle \lambda_j, \lambda_k \rangle^2\} \mid \{\lambda_j\}_{j \neq k}]}{\mathbb{E}_{\mathcal{G}_k}[\exp\{-\frac{1}{2\nu_\lambda} \sum_{j \neq k} \langle \lambda_j, \lambda_k \rangle^2\} \mid \{\lambda_j\}_{j \neq k}]} \\
&= \lim_{m \rightarrow \infty} \int_{\mathbb{R}^m} \exp\{i \frac{|T|}{m} U(\vec{t}^*)^\top \lambda_k(\vec{t}^*)\} (2\pi)^{-\frac{1}{2}} \det[C_k(\vec{t}^*, \vec{t}^*)^{-1} + \frac{|T|^2}{\nu_\lambda m^2} \Lambda_{-k}(\vec{t}^*) \Lambda_{-k}(\vec{t}^*)^\top]^{-\frac{1}{2}} \\
&\quad \times \exp\left\{-\frac{1}{2} \lambda_j(\vec{t}^*)^\top (C_k(\vec{t}^*, \vec{t}^*)^{-1} + \frac{|T|^2}{\nu_\lambda m^2} \Lambda_{-k}(\vec{t}^*) \Lambda_{-k}(\vec{t}^*)^\top) \lambda_j(\vec{t}^*)\right\} d\lambda_k(\vec{t}^*) \\
&= \lim_{m \rightarrow \infty} \exp\left\{-\frac{1}{2} \frac{|T|^2}{m^2} U(\vec{t}^*)^\top (C_k(\vec{t}^*, \vec{t}^*)^{-1} + \frac{|T|^2}{\nu_\lambda m^2} \Lambda_{-k}(\vec{t}^*) \Lambda_{-k}(\vec{t}^*)^\top)^{-1} U(\vec{t}^*)\right\}
\end{aligned} \tag{19}$$

$$\begin{aligned}
&= \lim_{m \rightarrow \infty} \exp\left\{-\frac{1}{2} \frac{|T|^2}{m^2} U(\vec{t}^*)^\top \left(C_k(\vec{t}^*, \vec{t}^*) - \frac{|T|}{m} C_k(\vec{t}^*, \vec{t}^*) \Lambda_{-k}(\vec{t}^*)\right.\right. \\
&\quad \left.\left. \times (\nu_\lambda I_{K-1} + \frac{|T|^2}{m^2} \Lambda_{-k}(\vec{t}^*)^\top C_k(\vec{t}^*, \vec{t}^*) \Lambda_{-k}(\vec{t}^*))^{-1} \frac{|T|}{m} \Lambda_{-k}(\vec{t}^*)^\top C_k(\vec{t}^*, \vec{t}^*)\right) U(\vec{t}^*)\right\}
\end{aligned} \tag{20}$$

$$= \exp\left\{-\frac{1}{2} \int_{\mathcal{T}} \int_{\mathcal{T}} C_k^{\nu_\lambda}(s, s') U(s) U(s') ds ds'\right\}, \tag{21}$$

where the matrix inversion from Equations (19) to (20) is computed via the Woodbury's formula (Harville 1998). In Equation (21), the characteristic functional of  $\lambda_k \mid \{\lambda_j\}_{j \neq k}$  coincides with the characteristic functional of a zero-mean Gaussian process with covariance function  $C_k^{\nu_\lambda}(\cdot, \cdot)$ , as desired.  $\square$

**Proposition A.5.**  $\lambda_k \mid \{\lambda_j\}_{j \neq k}$  converges in distribution to  $\lambda_k^\perp \mid \{\lambda_j\}_{j \neq k}$  as  $\nu_\lambda \rightarrow 0$ .

*Proof.* Under the assumption that  $H$  is a positive definite matrix, it follows that  $\lim_{\nu_\lambda \rightarrow 0} (\nu_\lambda I_{K-1} +$

$H)^{-1} = H^{-1}$ . Consider,

$$\begin{aligned}
\lim_{\nu_\lambda \rightarrow 0} \mathbb{E}_{\mathcal{N}_k} [\exp \{i \langle U, \lambda_k \rangle\} \mid \{\lambda_j\}_{j \neq k}] &= \lim_{\nu_\lambda \rightarrow 0} \exp \left\{ -\frac{1}{2} \int_{\mathcal{T}} \int_{\mathcal{T}} C_k^{\nu_\lambda}(s, s') U(s) U(s') ds ds' \right\} \\
&= \exp \left\{ -\frac{1}{2} \int_{\mathcal{T}} \int_{\mathcal{T}} C_k(s, s') U(s) U(s') ds ds' \right\} \\
&\times \lim_{\nu_\lambda \rightarrow 0} \exp \left\{ \frac{1}{2} \left( \int_{\mathcal{T}} U(s) h(s) ds \right)^\top (\nu_\lambda I_{K-1} + H)^{-1} \left( \int_{\mathcal{T}} U(s') h(s') ds' \right) \right\} \\
&= \exp \left\{ -\frac{1}{2} \int_{\mathcal{T}} \int_{\mathcal{T}} C_k(s, s') U(s) U(s') ds ds' \right\} \\
&\times \exp \left\{ \frac{1}{2} \left( \int_{\mathcal{T}} U(s) h(s) ds \right)^\top H^{-1} \left( \int_{\mathcal{T}} U(s') h(s') ds' \right) \right\} \\
&= \exp \left\{ -\frac{1}{2} \int_{\mathcal{T}} \int_{\mathcal{T}} C_{\Lambda(-k)}^\perp(s, s') U(s) U(s') ds ds' \right\}.
\end{aligned}$$

□

**Proposition A.6.** *Assuming  $\{\lambda_1, \dots, \lambda_K\} \sim \mathcal{N}$  with  $\mathcal{N}$ ,  $\langle \lambda_j, \lambda_k \rangle \mid \{\lambda_j\}_{j \neq k}$  converges in probability to 0 for any  $j \neq k$  as  $\nu_\lambda \rightarrow 0$ .*

*Proof.* First, consider

$$\begin{aligned}
\mathbb{E}_{\mathcal{N}_k} \left[ \int_{\mathcal{T}} \int_{\mathcal{T}} |\lambda_k(s) \lambda_k(s') \lambda_j(s) \lambda_j(s')| ds ds' \mid \{\lambda_j\}_{j \neq k} \right] &= \\
\mathbb{E}_{\mathcal{N}_k} [\|\lambda_j \lambda_k\|_1^2 \mid \{\lambda_j\}_{j \neq k}] & \tag{22}
\end{aligned}$$

$$\begin{aligned}
&\leq \|\lambda_j\|_2^2 \mathbb{E}_{\mathcal{N}_k} [\|\lambda_k\|_2^2 \mid \{\lambda_j\}_{j \neq k}] \\
&= \|\lambda_j\|_2^2 \int_{\mathbb{T}} \mathbb{E}_{\mathcal{N}_k} [\lambda_k(s)^2 \mid \{\lambda_j\}_{j \neq k}] ds \\
&= \|\lambda_j\|_2^2 \int_{\mathbb{T}} C_k^{\nu_\lambda}(s, s) ds \\
&\leq \|\lambda_j\|_2^2 \int_{\mathbb{T}} C_k(s, s) ds \tag{23}
\end{aligned}$$

Assuming that the covariance functions of the parent Gaussian Processes are defined so that

sample paths are almost surely continuous, Equation (23) is almost surely finite (Marcus & Shepp 1972). This implies that the expectation and integration operations in the left hand side of Equation (22) can be interchanged, by Fubini's theorem.

Define  $e_j$  to be a binary vector of length  $K - 1$  that satisfies  $\lambda_j(t) = e_j^\top \Lambda_{(-k)}(t)$ . For any  $\epsilon > 0$ , by Markov's inequality,

$$\begin{aligned}
\lim_{\nu_\lambda \rightarrow 0} P_{\mathcal{N}_k}(|\langle \lambda_j, \lambda_k \rangle| > \epsilon | \{\lambda_j\}_{j \neq k}) &\leq \lim_{\nu_\lambda \rightarrow 0} \frac{1}{\epsilon^2} \mathbb{E}_{\mathcal{N}_k} [|\langle \lambda_j, \lambda_k \rangle|^2 | \{\lambda_j\}_{j \neq k}] \\
&= \lim_{\nu_\lambda \rightarrow 0} \frac{1}{\epsilon^2} \mathbb{E}_{\mathcal{N}_k} \left[ \int_{\mathcal{T}} \int_{\mathcal{T}} \lambda_k(s) \lambda_k(s') \lambda_j(s) \lambda_j(s') ds ds' | \{\lambda_j\}_{j \neq k} \right] \\
&= \lim_{\nu_\lambda \rightarrow 0} \frac{1}{\epsilon^2} \int_{\mathcal{T}} \int_{\mathcal{T}} \mathbb{E}_{\mathcal{N}_k} [\lambda_k(s) \lambda_k(s') \lambda_j(s) \lambda_j(s') | \{\lambda_j\}_{j \neq k}] ds ds' \\
&= \lim_{\nu_\lambda \rightarrow 0} \frac{1}{\epsilon^2} \int_{\mathcal{T}} \int_{\mathcal{T}} C_k^{\nu_\lambda}(s, s') \lambda_j(s) \lambda_j(s') ds ds' \\
&= \lim_{\nu_\lambda \rightarrow 0} \frac{1}{\epsilon^2} (e_j^\top H e_j - e_j^\top H (\nu_\lambda I_{K-1} + H)^{-1} H e_j) = 0.
\end{aligned}$$

□

**Proposition A.7.**  $\eta_k$  converges in distribution to  $(I_n - \frac{1}{n} 1_n 1_n^\top) N(0, I_n)$  as  $\nu_\eta \rightarrow 0$ .

*Proof.* First notice,  $(I_n - \frac{1}{n} 1_n 1_n^\top) N(0, I_n) = N(0, (I_n - \frac{1}{n} 1_n 1_n^\top))$  in distribution, since  $(I_n - \frac{1}{n} 1_n 1_n^\top)$  is a symmetric idempotent matrix. Next, for any  $\epsilon > 0$ , choose  $\nu_\eta < \frac{\epsilon n^2}{\|1_n 1_n^\top\|_2}$ , and consider

$$\begin{aligned}
\|\text{var}(\eta_k) - (I_n - \frac{1}{n} 1_n 1_n^\top)\|_2 &= \frac{\nu_\eta}{n \nu_\eta + n^2} \|1_n 1_n^\top\|_2 \\
&< \frac{\nu_\eta}{n^2} \|1_n 1_n^\top\|_2 < \epsilon.
\end{aligned}$$

Hence,  $\text{var}(\eta_k) \rightarrow (I_n - \frac{1}{n} J)$  as  $\nu_\eta \rightarrow 0$ . Finally, for  $s \in \mathbb{R}^n$ , consider the characteristic



function of  $\eta_{\cdot k}$ ,

$$\begin{aligned}\lim_{\nu_\eta \rightarrow 0} \mathbb{E}[\exp(is^\top \eta_{\cdot k})] &= \lim_{\nu_\eta \rightarrow 0} \exp\left(-\frac{1}{2}s^\top \text{var}(\eta_{\cdot k})s\right) \\ &= \exp\left(-\frac{1}{2}s^\top (I_n - \frac{1}{n}1_n 1_n^\top)s\right),\end{aligned}$$

as desired. □

## B Additional Prior Illustration Figures

In this section, we illustrate the role of the length-scale and scale parameters of the conditional prior from Section 2.3 in the main paper. Panel (a) of Figure 6 again displays the value of  $\lambda_1$  on which  $\lambda_2 \mid \lambda_1$  is conditioned.

Figure 6 shows realizations from the prior with  $\tau_2^2 = 1, \nu_\lambda = 0.0001$  fixed, while  $l_2^2 = 0.001, 0.01, 0.1, 1$  varies in panels (d)-(g). Notice, as the length-scale parameter increases, the realizations become more smooth. When the realizations are relatively smooth, in panels (c)&(d), the variance shrinks around  $t \approx .65$ . This feature is present because of the prior's need to offset the extrema of  $\lambda_1$  to enforce orthogonality between the two functions. When the realizations are relatively rough, the shrinking of the variance of  $\lambda_2$  is less evident, since rougher functions tend to be close to orthogonal than smoother ones. Panel (b) of Figure 6 shows a boxplot of the inner product between  $\lambda_1$  and 1000 realizations of  $\lambda_2$  for the different values of the length-scale parameter. Varying  $l_2^2$  does not appear to have an effect on the inner product between  $\lambda_1$  and the realizations of  $\lambda_2 \mid \lambda_1$ .

Figure 6 shows realizations from the prior with  $l_2^2 = .1, \nu_\lambda = 0.0001$  fixed, and  $\tau_2^2 = 0.25, 0.5, 1, 2$  varying in panels (h)-(k). Varying this parameter changes the spread of the realizations, more drastically outside of the region where  $t \approx .65$ . Panel (c) of Figure 6 shows a boxplot of the inner product between  $\lambda_1$  and 1000 realizations of  $\lambda_2 \mid \lambda_1$  for the

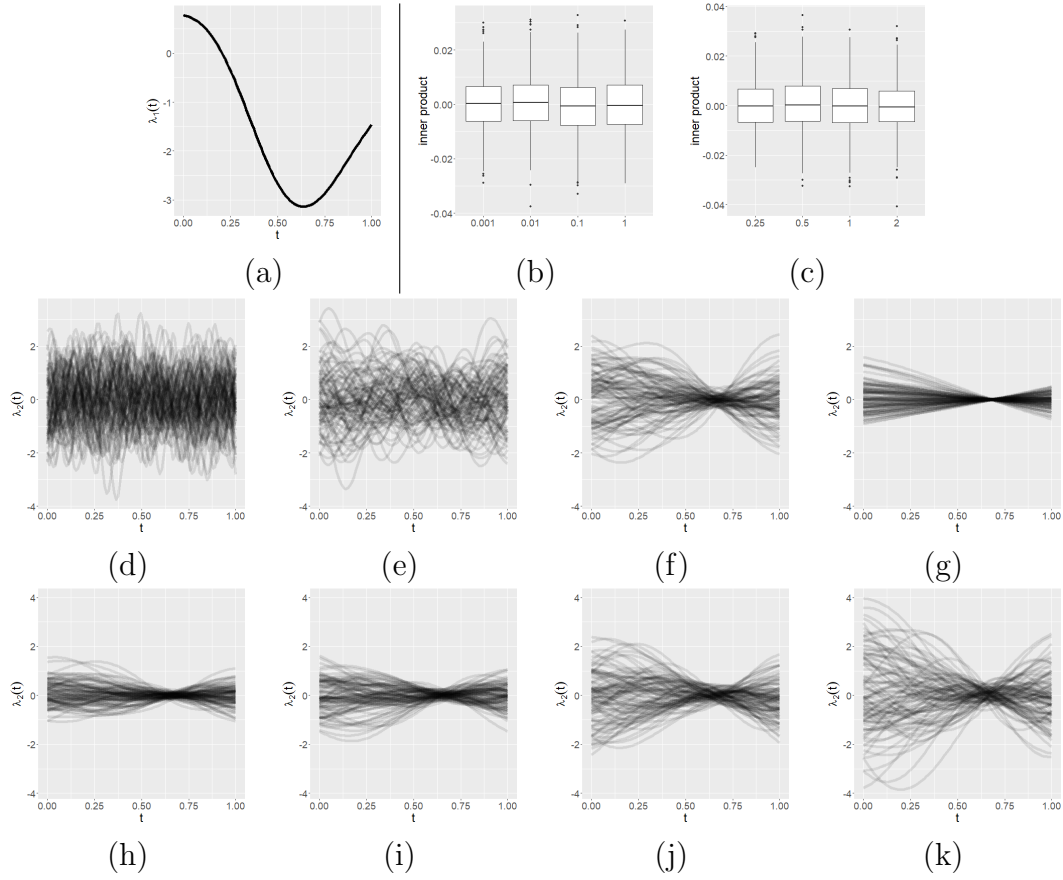


Figure 6: (a) The value of  $\lambda_1$  on which  $\lambda_2$  is conditioned. Boxplots of 1000 realizations of  $\langle \lambda_1, \lambda_2 \rangle$ , with  $\lambda_2 \mid \lambda_1 \sim \text{GP}(0, C_2^{\nu_\lambda}(\cdot, \cdot))$  (b)  $\tau_2^2 = 1$ ,  $\nu_\lambda = 0.0001$  are fixed as  $l_2 = 0.001, 0.01, 0.1, 1$  varies, (c)  $l_2 = 0.01$ ,  $\nu_\lambda = 0.0001$  are fixed as  $\tau_2^2 = 0.25, 0.5, 1, 2$  varies. Realizations of  $\lambda_2 \mid \lambda_1 \sim \text{GP}(0, C_2^{\nu_\lambda}(\cdot, \cdot))$  with (d)-(g)  $\tau_2^2 = 1, \nu_\lambda = 0.0001$  fixed, while  $l_2^2 = 0.001, l_2^2 = 0.01, l_2^2 = 0.1, l_2^2 = 1$  and with (h)-(k)  $l_2^2 = .1, \nu_\lambda = 0.0001$  fixed, while  $\tau_2^2 = 0.25, \tau_2^2 = 0.5, \tau_2^2 = 1, \tau_2^2 = 2$ .

different values of the scale parameter. Again, varying  $\tau_2^2$  does not appear to have an effect on the inner product between the  $\lambda_1$  and the realizations of  $\lambda_2 \mid \lambda_1$ .

## C Sensitivity Analysis For $\nu_\lambda$

While the sensitivity of the prior on  $\nu_\lambda$  is discussed at length in the main paper, we focus on the sensitivity of the posterior on  $\nu_\lambda$  for a simulated dataset in this section. Figure 7 panel (a) shows a simulated dataset that was generated according to the functional factor analysis observation model presented in the main paper, with  $K = 2$ . Panel (b) shows the

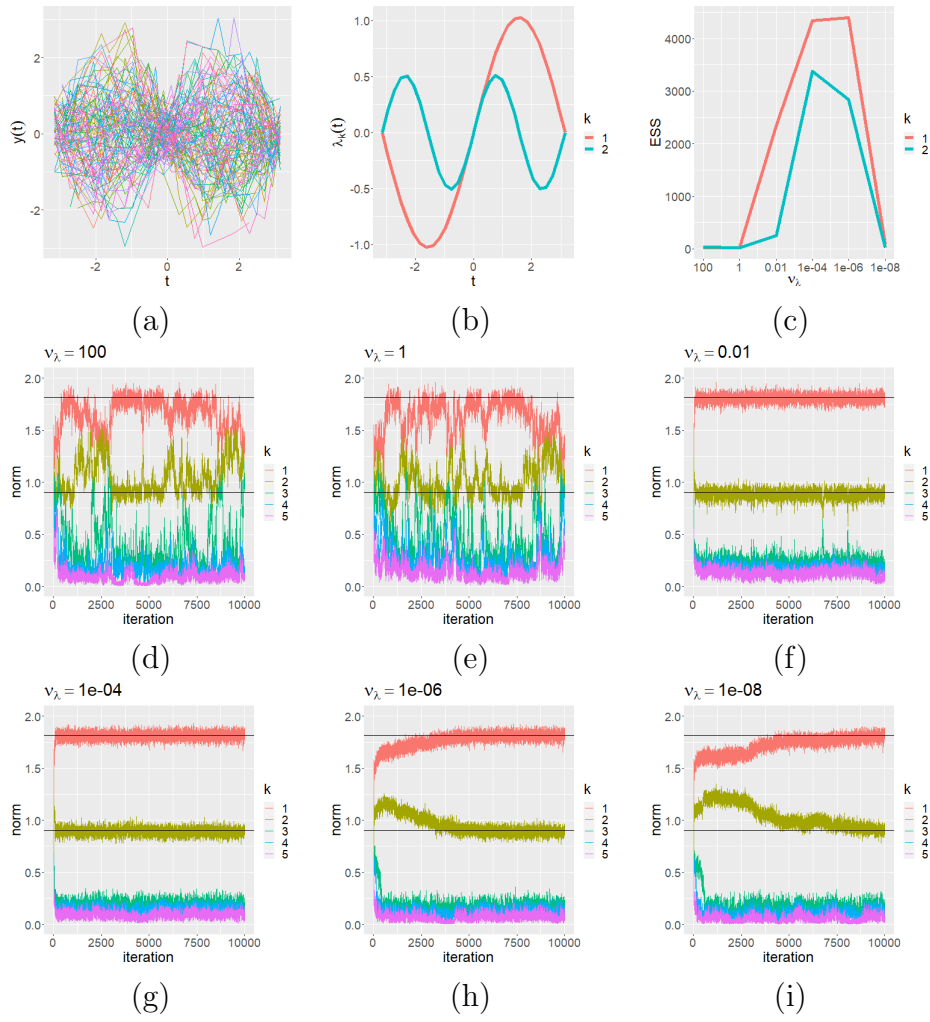


Figure 7: (a) Simulated observations. (b) Functional factor loadings that underlie the observations. (c) Effective sample size (ESS) of  $\|\lambda_k\|_2$ ,  $k = 1, 2$  for different values of  $\nu_\lambda$ . Trace plots of  $\|\lambda_k\|_2$ ,  $k = 1, \dots, 5$  for (d)  $\nu_\lambda = 100$ , (e)  $\nu_\lambda = 1$ , (f)  $\nu_\lambda = 0.01$ , (g)  $\nu_\lambda = 1e - 04$ , (h)  $\nu_\lambda = 1e - 06$ , (i)  $\nu_\lambda = 1e - 08$ .

2 functional factor loadings that underlie the observations in panel (a). These are specified as the orthogonal functions  $\lambda_1(t) := \sin(t)$  and  $\lambda_2(t) := \frac{1}{2} \sin(2t)$ . To study the effects of  $\nu_\lambda$  on posterior inference, we run several Markov chain Monte Carlo implementations of our model at different values of  $\nu_\lambda = 100, 1, 0.01, 1e - 04, 1e - 06, 1e - 08$ . During these different implementations we fix  $K = 5$ , and the initialization and the seed for the psuedo-random number generator to simulate Markov chain Monte Carlo samples from the target posterior. Panels (d)-(i) of Figure 7 show trace plots of 10,000 posterior samples of  $\|\lambda_k\|_2$ ,  $k = 1, \dots, 5$ , with the true values of  $\|\lambda_k\|_2$ ,  $k = 1, 2$  shown as black horizontal lines.

In the setting where  $\nu_\lambda$  is large, as in panels (d)&(e), the model is not able to properly infer the loadings, and the inferred loadings split the true factors as indicated by the norms of the Markov chain Monte Carlo samples failing to converge. At the other extreme, panels (h)&(i) show posterior samples of loadings that mix slowly, and take a large number of iterations to converge to a posterior mode. Panel (c) shows the effective sample size of the posterior samples of  $\|\lambda_k\|_2$ ,  $k = 1, 2$  after the first 5,000 Markov chain Monte Carlo iterations. The effective sample size of  $\|\lambda_k\|_2$ ,  $k = 1, 2$  is small for  $\nu_\lambda = 100$  and 1 because of factor splitting, while the effective sample size for  $\nu_\lambda = 1e - 08$  is small because of slow mixing. A value of  $\nu_\lambda = 1e - 04$  balances these two extremes and has a relatively large effective sample size.

## D Markov chain Monte Carlo Implementation

We concisely restate the likelihood and prior distributions in hierarchical model notation.

Our hierarchical functional factor analysis model is specified as follows,

$$\begin{aligned}
y_i \mid \mu(\vec{t}), \lambda_1(\vec{t}), \dots, \lambda_K(\vec{t}), \eta_i &\sim N_{m_i}(O_i \mu(\vec{t}) + O_i(\lambda_1(\vec{t}), \dots, \lambda_K(\vec{t}))^\top \eta_i, \sigma^2 I_{m_i}), \quad i = 1 \dots, n \\
\mu \mid l_\mu, \tau_\mu^2 &\sim \text{GP}(0, C_\mu(\cdot, \cdot)), \quad (l_\mu^2)^{-1} \sim \text{gamma}(\alpha_\mu, \beta_\mu), \quad \tau_\mu^2 \sim \text{half-normal}(\gamma_\mu) \\
\lambda_k \mid l_k, \tau_k^2, \Lambda_{(-k)} &\sim \text{GP}(0, C_k^{\nu_\lambda}(\cdot, \cdot)), \quad \eta_{\cdot k} \mid \psi_k \sim N(0, \psi_k(I_n + \frac{1}{\nu_\eta} \mathbf{1}_n \mathbf{1}_n^\top)^{-1}), \quad k = 1, \dots, K \\
(l_k^2)^{-1} &\sim \text{gamma}(\alpha_\lambda, \beta_\lambda), \quad \tau_k^2 \sim \text{half-normal}(\gamma_\lambda), \quad (\psi_k)^{-1} \sim \text{gamma}(\alpha_\eta, \beta_\eta), \quad k = 1, \dots, K \\
(\sigma^2)^{-1} &\sim \text{gamma}(\alpha_\sigma, \beta_\sigma).
\end{aligned}$$

Our hierarchical generalized functional factor analysis extension for binary functional data is

$$\begin{aligned}
z_i(\vec{t}_i) &= \begin{cases} 1, & z_i^*(\vec{t}_i) > 0, \\ 0, & \text{otherwise, } i = 1, \dots, n, \end{cases} \\
z_i^*(\vec{t}_i) \mid \mu(\vec{t}), \lambda_1(\vec{t}), \dots, \lambda_K(\vec{t}), \eta_i &\text{ind} \sim N_{m_i}(O_i \mu(\vec{t}) + O_i(\lambda_1(\vec{t}), \dots, \lambda_K(\vec{t}))^\top \eta_i, I_{m_i}), \quad i = 1 \dots, n \\
\mu \mid l_\mu, \tau_\mu^2 &\sim \text{GP}(0, C_\mu(\cdot, \cdot)), \quad (l_\mu^2)^{-1} \sim \text{gamma}(\alpha_\mu, \beta_\mu), \quad \tau_\mu^2 \sim \text{half-normal}(\gamma_\mu) \\
\lambda_k \mid l_k, \tau_k^2, \Lambda_{(-k)} &\sim \text{GP}(0, C_k^{\nu_\lambda}(\cdot, \cdot)), \quad \eta_k \mid \psi_k \sim N(0, \psi_k(I_n + \frac{1}{\nu_\eta} \mathbf{1}_n \mathbf{1}_n^\top)^{-1}), \quad k = 1, \dots, K \\
(l_k^2)^{-1} &\sim \text{gamma}(\alpha_\lambda, \beta_\lambda), \quad \tau_k^2 \sim \text{half-normal}(\gamma_\lambda), \quad (\psi_k)^{-1} \sim \text{gamma}(\alpha_\eta, \beta_\eta), \quad k = 1, \dots, K.
\end{aligned}$$

The  $\psi_k$  auxiliary parameters introduced in the priors for  $\eta_k$  govern prior variance following the parameter expansion approach of Ghosh & Dunson (2009), which introduced this technique in the context of multivariate latent factor models. Inference of the  $\psi_k$  parameters themselves is usually not of interest. Saved posterior samples of  $\psi_k$  are used to scale saved posterior samples of  $\lambda_k$  and  $\eta_k$ . This approach has been shown to diminish posterior dependence and lead to better Markov chain Monte Carlo mixing.

Throughout the algorithms presented in this section, we use the superscript *cur* and *can* to denote current and candidate states of parameters in the Markov chain, and use superscripted square brackets to denote saved parameter values. The notation  $\cdot \mid -$  is used to denote a parameter conditioned on all other parameters and the data.

For algorithm to sample parameters from functional factor analysis model presented in Algorithm 1, the full conditional distribution of  $\mu(\vec{t})$  is

$$\begin{aligned}
\mu(\vec{t}) \mid - &\sim N(\mathbb{E}[\mu(\vec{t}) \mid -], \mathbb{V}[\mu(\vec{t}) \mid -]), \\
\mathbb{V}[\mu(\vec{t}) \mid -] &= \left( C_\mu^{-1}(\vec{t}, \vec{t}) + \frac{1}{\sigma^2} \sum_{i=1}^n O_i^\top O_i \right)^{-1} \\
\mathbb{E}[\mu(\vec{t}) \mid -] &= \frac{1}{\sigma^2} \mathbb{V}[\mu(\vec{t}) \mid -] \sum_{i=1}^n \left( O_i^\top y_i(\vec{t}_i) - O_i^\top O_i \sum_{k=1}^K \eta_{i,k} \lambda_k(\vec{t}) \right).
\end{aligned} \tag{24}$$

---

**Algorithm 1** Metropolis-within-Gibbs for Functional Factor Analysis

---

- 1: Randomly initialize current states of all parameters using their prior distribution
- 2: **for** iter = 1 : N **do**
- 3:   Draw  $\mu^{cur}(\vec{t}) \mid - \sim \pi(\mu(\vec{t}) \mid -)$  from Equation (24)
- 4:   Propose  $l_\mu^{can} \sim N(l_\mu^{cur}, \Sigma_{l_\mu}^{prop})$
- 5:   Compute  $\alpha_{l_\mu} := \frac{\pi(\mu^{cur}(\vec{t}) \mid l_\mu^{can}, \tau_\mu^{2,cur})\pi(l_\mu^{can})}{\pi(\mu^{cur}(\vec{t}) \mid l_\mu^{cur}, \tau_\mu^{2,cur})\pi(\tau_\mu^{2,cur})}$
- 6:   If  $\text{unif}(0, 1) < \alpha_{l_\mu}$ , set  $l_\mu^{cur} = l_\mu^{can}$
- 7:   Propose  $\tau_\mu^{2,can} \sim N(\tau_\mu^{2,cur}, \Sigma_{\tau_\mu^2}^{prop})$
- 8:   Compute  $\alpha_{\tau_\mu^2} := \frac{\pi(\mu^{cur}(\vec{t}) \mid l_\mu^{cur}, \tau_\mu^{2,can})\pi(\tau_\mu^{2,can})}{\pi(\mu^{cur}(\vec{t}) \mid l_\mu^{cur}, \tau_\mu^{2,cur})\pi(\tau_\mu^{2,cur})}$
- 9:   If  $\text{unif}(0, 1) < \alpha_{\tau_\mu^2}$ , set  $\tau_\mu^{2,cur} = \tau_\mu^{2,can}$
- 10:   **for** k in 1 : K **do**
- 11:     Draw  $\lambda_k^{cur}(\vec{t}) \mid - \sim \pi(\lambda_k(\vec{t}) \mid -)$  from Equation (25)
- 12:     Propose  $l_k^{can} \sim N(l_k^{cur}, \Sigma_{l_k}^{prop})$
- 13:     Compute  $\alpha_{l_k} := \frac{\pi(\lambda_k^{cur}(\vec{t}) \mid l_k^{can}, \tau_k^{2,cur})\pi(l_k^{can})}{\pi(\lambda_k^{cur}(\vec{t}) \mid l_k^{cur}, \tau_k^{2,cur})\pi(\tau_k^{2,cur})}$
- 14:     If  $\text{unif}(0, 1) < \alpha_{l_k}$ , set  $l_k^{cur} = l_k^{can}$
- 15:     Propose  $\tau_k^{2,can} \sim N(\tau_k^{2,cur}, \Sigma_{\tau_k^2}^{prop})$
- 16:     Compute  $\alpha_{\tau_k^2} := \frac{\pi(\lambda_k^{cur}(\vec{t}) \mid l_k^{cur}, \tau_k^{2,can})\pi(\tau_k^{2,can})}{\pi(\lambda_k^{cur}(\vec{t}) \mid l_k^{cur}, \tau_k^{2,cur})\pi(\tau_k^{2,cur})}$
- 17:     If  $\text{unif}(0, 1) < \alpha_{\tau_k^2}$ , set  $\tau_k^{2,cur} = \tau_k^{2,can}$
- 18:     Draw  $\eta_{\cdot k}^{cur} \mid - \sim \pi(\eta_{\cdot k} \mid -)$  from Equation (26)
- 19:     Draw  $\psi_k^{cur} \mid - \sim \pi(\psi_k \mid -)$  from Equation (27)
- 20:   Draw  $\sigma^{2,cur} \mid - \sim \pi(\sigma^2 \mid -)$  from Equation (28)
- 21:   Save

$$\begin{aligned} & \mu^{[iter]}(\vec{t}), l_\mu^{[iter]}, \tau_\mu^{2,[iter]} \{ \lambda_k(\vec{t})^{[iter]}, l_k^{[iter]}, \tau_k^{2,[iter]}, \eta_{\cdot k}^{[iter]}, \psi_k^{[iter]} \}_{k=1}^K, \sigma^{2,[iter]} \\ & := \mu^{cur}(\vec{t}), l_\mu^{cur}, \tau_\mu^{2,cur} \{ \lambda_k(\vec{t})^{cur}, l_k^{cur}, \tau_k^{2,cur}, \eta_{\cdot k}^{cur}, \psi_k^{cur} \}_{k=1}^K, \sigma^{2,cur} \end{aligned}$$


---

The full conditional distribution of  $\lambda_k(\vec{t})$ ,  $k = 1, \dots, K$  is

$$\begin{aligned} \lambda_k(\vec{t}) \mid - & \sim N(\mathbb{E}[\lambda_k(\vec{t}) \mid -], \mathbb{V}[\lambda_k(\vec{t}) \mid -]), \\ \mathbb{V}[\lambda_k(\vec{t}) \mid -] & = (C_k^{-1}(\vec{t}, \vec{t}) + \frac{1}{\nu_\lambda} W \Lambda_{(-k)}(\vec{t}) \Lambda_{(-k)}(\vec{t})^\top W + \frac{1}{\sigma^2} \sum_{i=1}^n \eta_{i,k}^2 O_i^\top O_i)^{-1} \\ \mathbb{E}[\lambda_k(\vec{t}) \mid -] & = \frac{1}{\sigma^2} \mathbb{V}[\lambda_k(\vec{t}) \mid -] \sum_{i=1}^n (\eta_{i,k} O_i^\top y_i(\vec{t}_i) - O_i^\top O_i \mu(\vec{t}) - O_i^\top O_i \sum_{j \neq k} \eta_{i,j} \lambda_j(\vec{t})). \end{aligned} \tag{25}$$

The full conditional distribution of  $\eta_k$ ,  $k = 1, \dots, K$  is

$$\begin{aligned}\eta_k | - &\sim N(\mathbb{E}[\eta_k | -], \mathbb{V}[\eta_k | -]), \\ \mathbb{V}[\eta_k | -] &= \left( \text{diag}(\lambda_k(\vec{t})^\top O_i^\top O_i \lambda_k(\vec{t}))_{i=1}^n + \frac{1}{\psi_k} (I_n + \frac{1}{\nu_\eta} \mathbf{1}_n \mathbf{1}_n^\top) \right)^{-1} \\ \mathbb{E}[\eta_k | -] &= \frac{1}{\sigma^2} \mathbb{V}[\eta_k | -] \left[ (y_i(\vec{t}_i) - O_i \mu(\vec{t}) - O_i \sum_{j \neq k} \eta_{i,j} \lambda_j(\vec{t}))^\top O_i \lambda_k(\vec{t}) \right]_{i=1}^n,\end{aligned}\tag{26}$$

where  $\text{diag}(\cdot)_{i=1}^n$  denotes a diagonal matrix with diagonal elements given by the argument, and  $[\cdot]_{i=1}^n$  is a vector with elements given by the argument.

The full conditional distribution of  $\psi_k$ ,  $k = 1, \dots, K$  is

$$(\psi_k)^{-1} | - \sim \text{gamma}\left(\alpha_\eta + \frac{n}{2}, \beta_\eta \frac{1}{2} \eta_{\cdot k}^\top (I_n + \frac{1}{\nu_\eta} \mathbf{1}_n \mathbf{1}_n^\top)^{-1} \eta_{\cdot k}\right)\tag{27}$$

The full conditional distribution of  $\sigma^2$  is

$$\begin{aligned}(\sigma^2)^{-1} | - &\sim \text{gamma}\left(\alpha_\sigma + \frac{1}{2} \sum_{i=1}^n m_i, \right. \\ &\left. \beta_\sigma + \frac{1}{2} \sum_{i=1}^n \sum_{j=1}^{m_i} (y_i(t_{i,j}) - \mu(t_{i,j}) + \sum_{k=1}^K \eta_{i,k} \lambda_k(t_{i,j}))^2\right).\end{aligned}\tag{28}$$

A Metropolis-within-Gibbs algorithm for our generalized functional factor analysis approach for binary functional data is presented in Algorithm 2. The latent variable formulation of the probit model leads to a simple step for sampling the latent processes  $z_i^*$ ,  $i = 1, \dots, n$  as described in Albert & Chib (1993). Conditioning on the latent processes, the sampling of the model parameters is similar to the functional factor analysis setting.

---

**Algorithm 2** Metropolis-within-Gibbs for Generalized Functional Factor Analysis

---

- 1: Randomly initialize current states of all parameters using their prior distribution
- 2: **for** iter = 1 : N **do**
- 3:     **for** i = 1 : n **do**
- 4:         **for** j = 1 :  $m_i$  **do**
- 5:             Draw  $z_i^{*,cur}(t_{i,j}) \mid - \sim$ 
$$\begin{cases} \text{truncated-normal}_{(0,\infty)}(\mu^{cur}(t_{i,j}) + \sum_{k=1}^K \eta_{i,k}^{cur} \lambda_k^{cur}(t_{i,j}), 1), & z_i(t_{i,j}) = 1, \\ \text{truncated-normal}_{(-\infty,0)}(\mu^{cur}(t_{i,j}) + \sum_{k=1}^K \eta_{i,k}^{cur} \lambda_k^{cur}(t_{i,j}), 1), & z_i(t_{i,j}) = 0. \end{cases}$$
- 6:              $\mu^{cur}(\vec{t}), l_\mu^{cur}, \tau_\mu^{2,cur} \{ \lambda_k(\vec{t})^{cur}, l_k^{cur}, \tau_k^{2,cur}, \eta_{\cdot k}^{cur}, \psi_k^{cur} \}_{k=1}^K$  can be sampled using steps 3 - 19 of Algorithm 1, replacing  $y_i := z_i^*$ ,  $i = 1, \dots, n$  and  $\sigma^2 := 1$
- 7:             Save

$$\begin{aligned} & \mu^{[iter]}(\vec{t}), l_\mu^{[iter]}, \tau_\mu^{2,[iter]} \{ \lambda_k(\vec{t})^{[iter]}, l_k^{[iter]}, \tau_k^{2,[iter]}, \eta_{\cdot k}^{[iter]}, \psi_k^{[iter]} \}_{k=1}^K \\ & := \mu^{cur}(\vec{t}), l_\mu^{cur}, \tau_\mu^{2,cur} \{ \lambda_k(\vec{t})^{cur}, l_k^{cur}, \tau_k^{2,cur}, \eta_{\cdot k}^{cur}, \psi_k^{cur} \}_{k=1}^K \end{aligned}$$

---

## E Additional Simulated Examples

### E.1 Repeated Estimation and Coverage Simulations

In this subsection, we repeat the simulation examples presented in the main paper under slightly different data generating distributions with results in Figure 8<sup>2</sup>.

Panel (a) illustrates estimation performance for functional factor analysis when data are generated as in Section 4.1 from the main paper, except with smaller error variance,  $\sigma^2 = .25$ . Again, it appears that estimation performance deteriorates with sparsity level and relative to the NeMO method, the competitors generally have larger error. Panel (b) illustrates estimation performance for generalized functional factor analysis when data are generated as in Section 4.2 from the main paper, except with smaller scale parameter for the generalized functional factor loadings,  $\tau_\mu^2 = \tau_{\lambda_1}^2 = \tau_{\lambda_2}^2 = 1$ . Mean integrated squared error from NeMO is consistently below that of the others. Panel (c) displays coverage results in a latent factor regression setup where the data are generated as in Section 4.3 from the main paper, except with smaller error variance,  $\sigma^2 = .25$ . In this setting, all methods provide

---

<sup>2</sup>Abbreviations in figure legends: CG2010 - Crainiceanu & Goldsmith (2010); PP2009 - Peng & Paul (2009); WZSG2019 - Wrobel et al. (2019); YMW2005 - Yao et al. (2005); ZLLZ2021 - Zhong et al. (2021).



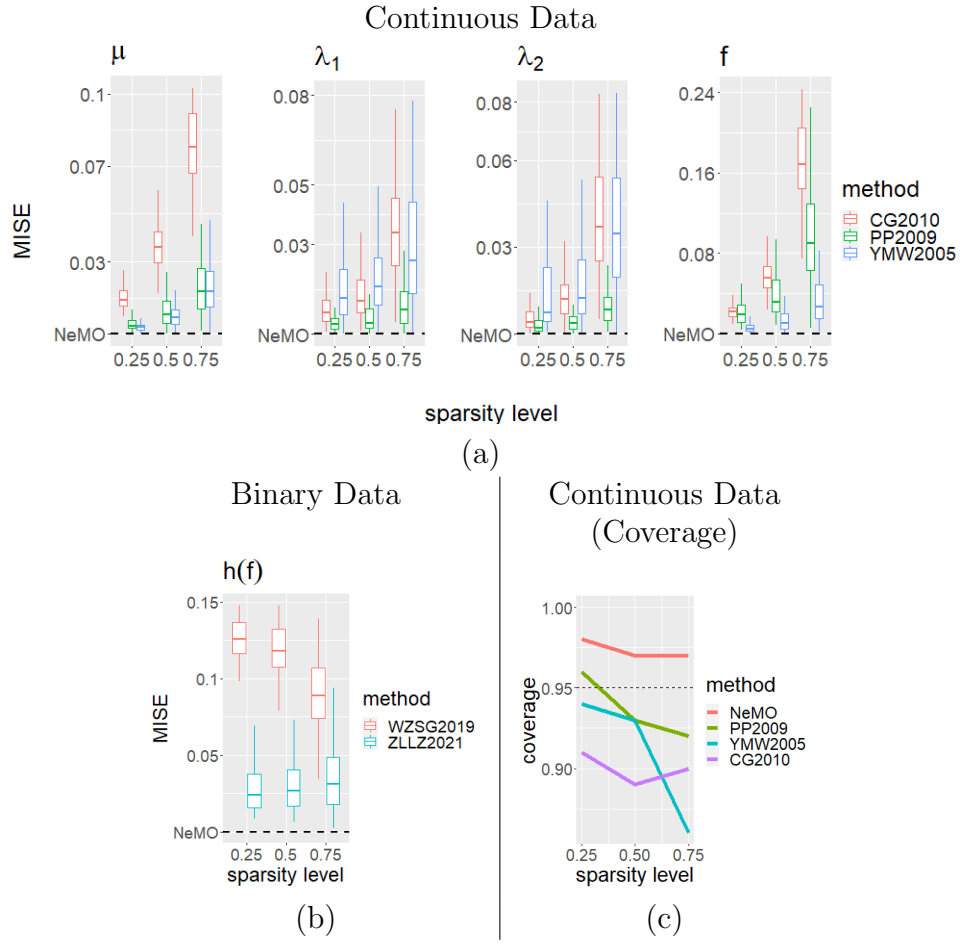


Figure 8: (a) & (b) Mean integrated squared error for estimated parameters at different sparsity levels in Gaussian and non-Gaussian settings, respectively. (c) Coverage of credible/confidence intervals for different methods at different sparsity levels in the latent factor regression setting.

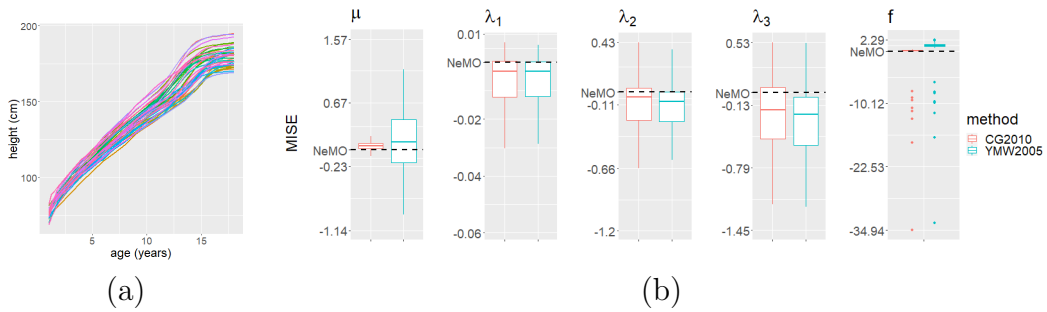


Figure 9: (a) Observed growth curves for  $n = 39$  male subjects in the Berkeley growth study. (b) Mean integrated squared error results of estimated model parameters.

reasonable coverage, except for that of Yao et al. (2005) in the high sparsity setting.

## E.2 Simulation Example under Model Misspecification

In this simulated example we generate data that replicate the variability in observations from the Berkeley growth study, described in (Ramsay & Silverman 2005). Panel (a) of Figure 9 displays the height in centimeters of the 39 male children in the study. Using the **fdapace** R package we inferred the components of an functional factor analysis model that implements the methodology of Yao et al. (2005), under the following observation model

$$y_i(\vec{t}) = \mu(\vec{t}) + (\lambda_1(\vec{t}), \dots, \lambda_K(\vec{t}))^\top \eta_i + \epsilon_i(\vec{t}), \quad i = 1, \dots, n. \quad (29)$$

The ages  $\vec{t}$  correspond to quarterly measurements in the first year of age, annual measurements from age two to age eight, then biannual measurements from age 8 to 18. The **fdapace** package selected  $K = 3$ , so that the estimated fraction of variance explained by the loadings is 95%. In this simulation, we sample independent Gaussian latent factors and additive error with variance estimated from **fdapace**, and plug estimates of the mean and factor loadings into the above observation model to generate functional datasets with variability similar to that of Figure 9(a). Using the simulated observations, we measure estimation performance of various methods using mean integrated squared error.

For the NeMO model, we use the posterior mean of  $\mu(\vec{t}) + (\lambda_1(\vec{t}), \dots, \lambda_K(\vec{t}))^\top \eta_i$  to produce an estimate of  $f_i$  based on 1,000 Markov chain Monte Carlo samples. In terms of other functional factor analysis methods, we compare to Yao et al. (2005), Peng & Paul (2009), and Crainiceanu & Goldsmith (2010) as in the main paper. We replicate the entire data generating mechanism 100 times for comparison. Panel (b) of Figure 9<sup>3</sup> shows mean integrated squared error results. The results from the Peng & Paul (2009) method is excluded from the figure because the mean integrated squared error was orders of magnitudes larger than the other three methods. The mean integrated squared error computed using NeMO, Yao et al. (2005), and Crainiceanu & Goldsmith (2010) estimates

---

<sup>3</sup>Abbreviations in figure legend: CG2010 - Crainiceanu & Goldsmith (2010); YMW2005 - Yao et al. (2005).

are all comparable. Occasionally, the NeMO model selects  $K < 3$ , which results in the mean integrated squared error to be larger than the competitors, although this only happened in 8 of the 100 replicates. Even in this realistic simulation setting under model misspecification, our functional factor analysis model using NeMO processes performs well compared with competing methods.

## F Additional Information for the Analysis of the Cebu Longitudinal Health and Nutrition Survey Dataset

### F.1 Hierarchical Model Formulation

In Section 5 of the main paper, we motivated a flexible model for weight of young children while accounting for scalar and longitudinal covariates. The observation model is restated as follows,

$$\begin{aligned} y_i(\vec{t}_i) &= O_i \mu(\vec{t}) + O_i (\lambda_1(\vec{t}), \dots, \lambda_K(\vec{t}))^\top \eta_i + O_i \sum_{j=1}^4 \int_T \beta_j(s, \vec{t}) z_{i,j}(s) ds + \epsilon_i(\vec{t}_i) \\ \eta_i &= \Theta x_i + \xi_i \end{aligned} \quad (31)$$

Similar to the hierarchical functional factor analysis model presented in section D, we specify the following model components:

$$\begin{aligned} \mu \mid l_\mu, \tau_\mu^2 &\sim \text{GP}(0, C_\mu(\cdot, \cdot)), \quad (l_\mu^2)^{-1} \sim \text{gamma}(\alpha_\mu, \beta_\mu), \quad \tau_\mu^2 \sim \text{half-normal}(\gamma_\mu) \\ \lambda_k \mid l_k, \tau_k^2, \Lambda_{(-k)} &\sim \text{GP}(0, C_k^{\nu_\lambda}(\cdot, \cdot)), \quad k = 1, \dots, K \\ (l_k^2)^{-1} &\sim \text{gamma}(\alpha_\lambda, \beta_\lambda), \quad \tau_k^2 \sim \text{half-normal}(\gamma_\lambda) \quad k = 1, \dots, K \\ \epsilon_i(\vec{t}_i) \mid \sigma^2 &\sim N(0, I_{m_i}), \quad i = 1 \dots, n, \quad (\sigma^2)^{-1} \sim \text{gamma}(\alpha_\sigma, \beta_\sigma). \end{aligned}$$

We incorporate scalar covariates,  $x_i$ , through the latent factors,  $\eta_i = Bx_i + \xi_i$ . For these model parameters, we assign

$$\begin{aligned}\Theta_{k,q} \mid \psi_k &\sim N(0, \psi_k), \quad q = 1, \dots, 4, \quad \xi_k \mid \psi_k \sim N(0, \psi_k(I_n + \frac{1}{\nu_\eta} \mathbf{1}_n \mathbf{1}_n^\top)^{-1}), \quad k = 1, \dots, K \\ (\psi_k)^{-1} &\sim \text{gamma}(\alpha_\xi, \beta_\xi), \quad k = 1, \dots, K\end{aligned}$$

As noted in the main paper, the longitudinal covariates are sparsely recorded. Based on initial EDA of the data, the illness indicator covariates,  $z_{i,2}, z_{i,3}, z_{i,4}$ ,  $i = 1, \dots, n$ , do not appear to have much structured variability across subjects. For model based imputation of these covariates, we model the probability of illness at time  $s$  as  $p(z_{i,j}(s) = 1) = \Phi(\mu^{z_j}(s))$ ,  $i = 1, \dots, n, j = 2, 3, 4$ . Alternatively, we do suspect that there is structured variability in the breastfeeding indicator  $z_{i,1}$ , given typical breastfeeding patterns and biological constraints. We model  $P(z_{i,1}(t) = 1) = \Phi(\mu^{z_1}(s) + (\lambda_1^z(s), \dots, \lambda_{K_z}^z(s))^\top \eta_i^z)$  as in the generalized functional factor analysis setting of our model. For these components, we assign

$$\begin{aligned}\mu^{z_j}(\vec{s}) \mid l_{\mu^{z_j}}, \tau_{\mu^{z_j}}^2 &\sim \text{GP}(0, C_{\mu^{z_j}}(\cdot, \cdot)), \quad j = 1, \dots, 4 \\ (l_{\mu^{z_j}}^2)^{-1} &\sim \text{gamma}(\alpha_{\mu^z}, \beta_{\mu^z}), \quad \tau_{\mu^{z_j}}^2 \sim \text{half-normal}(\gamma_{\mu^z}), \quad j = 1, \dots, 4 \\ \lambda_k^z \mid l_k^z, \tau_k^{2,z}, \Lambda_{(-k)}^z &\sim \text{GP}(0, C_{k^z}^\nu(\cdot, \cdot)), \quad \eta_{\cdot k}^z \mid \psi_k^z \sim N(0, \psi_k^z(I_n + \frac{1}{\nu_\eta} \mathbf{1}_n \mathbf{1}_n^\top)^{-1}), \\ (l_k^{2,z})^{-1} &\sim \text{gamma}(\alpha_{\lambda^z}, \beta_{\lambda^z}), \quad \tau_k^{2,z} \sim \text{half-normal}(\gamma_{\lambda^z}), \quad (\psi_k^z)^{-1} \sim \text{gamma}(\alpha_{\eta^z}, \beta_{\eta^z}), \\ k &= 1, \dots, K^z.\end{aligned}$$

For grid points where the covariates are not observed,  $s_{i,z_j}^{miss}$ ,  $j = 1, \dots, 4$ , values are imputed for  $z_{i,j}(s_{i,z_j}^{miss})$  based on the above models. These values are sampled throughout the Markov chain Monte Carlo algorithm to account for the uncertainty due to the missing data.

Finally, we can specify the model components for the functional linear model component (Ramsay & Dalzell 1991). Each  $\beta_{(s,t)}$  is represented via a basis expansion. For the historical

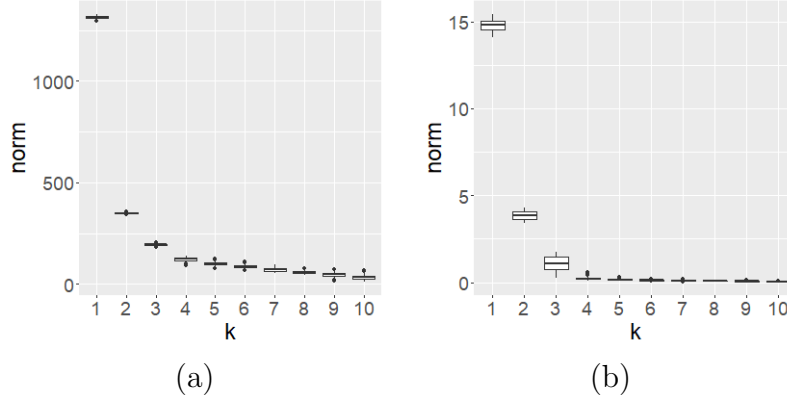


Figure 10: Scree plots that display boxplots of posterior samples of norms of factor loadings for the (a) weight and (b) breastfeeding trajectories of children in the Cebu Longitudinal Health and Nutritional Survey.

linear model component for the breastfeeding indicator, we use the tent basis described in Malfait & Ramsay (2003). We denote these basis elements with  $V_{p,1}(s, t)$ ,  $p = 1, \dots, P$ , so that  $\int_T \beta_1(s, t) z_{i,1}(s) ds = \sum_{p=1}^{P_1} \rho_{p,1} \int_T V_{p,1}(s, t) z_{i,1}(s) ds$ , where the integrals are approximated numerically based on the imputed breastfeeding indicator covariate. For the illness covariates, the integral form equates to  $\int_T \beta_j(s, t) z_{i,j}(s) ds = \beta_j(t) z_{i,j}(t)$ ,  $j = 2, 3, 4$  in the concurrent linear model (Hastie & Tibshirani 1993). We represent each with a b-spline basis,  $\beta_j(t) = \sum_{p=1}^{P_j} \rho_{p,j} V_{p,j}(t)$ . Inference for these model components is carried out through inference on the basis coefficients for which we specify

$$\rho_{p,j} \sim N(0, \tau_\rho^2), \quad p = 1, \dots, P_j, \quad j = 1, \dots, 4.$$

## F.2 Additional Figures for Posterior Inference

In the main paper, the inferential results for the analysis of the Cebu Longitudinal Health and Nutrition Survey are reported with  $K = 5$  and  $K^z = 3$ . These numbers of factors were selected based on the approach outlined in Section 3.4 of the main paper. Figure 10 displays scree plots of norms of inferred loadings for modeling weight and breastfeeding trajectories based on a larger number of latent factors. In both of these cases, the first few

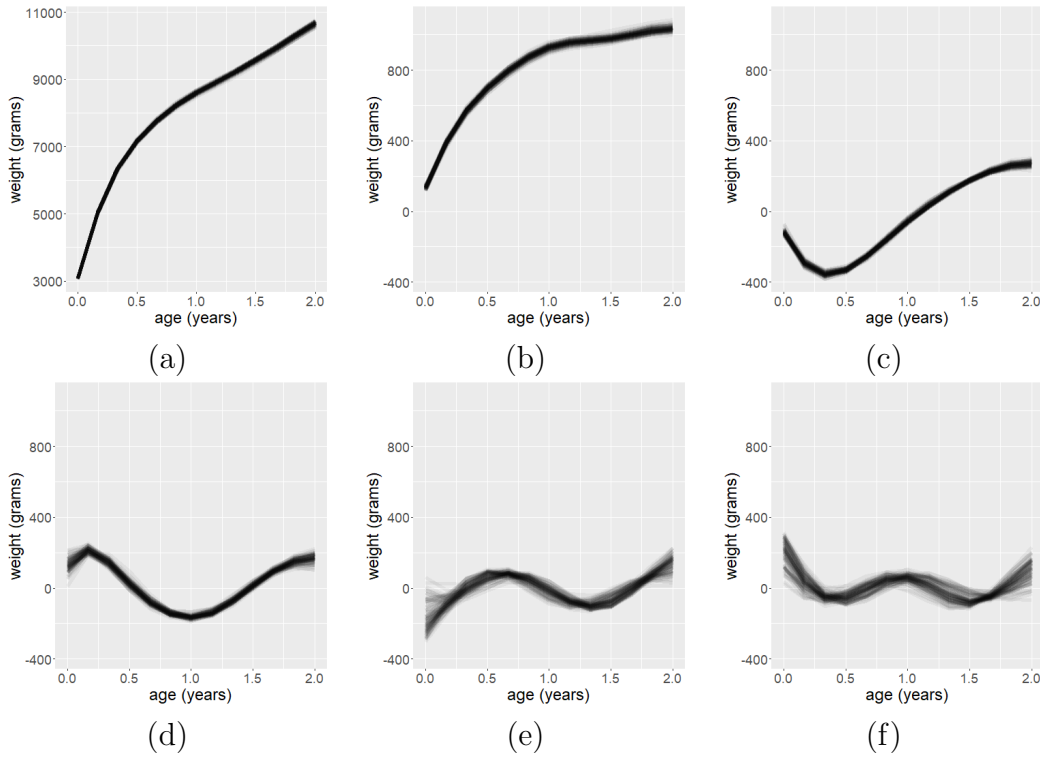


Figure 11: (a) Posterior samples of the mean process,  $\mu(\vec{t})$ , and (b)-(f) functional factor loadings,  $\lambda_1(\vec{t}), \dots, \lambda_5(\vec{t})$ , for weight measurements of children recorded in the Cebu Longitudinal Health and Nutrition Survey.

loadings are significantly larger in magnitude compared to trailing loadings.

Posterior samples of the mean process,  $\mu$ , and functional factor loadings,  $\lambda_1, \dots, \lambda_5$  are displayed in Figure 11 in panels (a) and (b)-(f), respectively. The mean process increases rapidly from age 0 to 6 months, then appears to behave nearly linearly from age 6 months to 2 years. The first loading shown in panel (b) captures subject specific deviations having roughly a similar shape as the mean. The latter loadings in panels (c)-(f) capture more intricate variability that is smaller in magnitude.

As discussed in the main paper, model based imputation is needed for the longitudinal covariates in order to compute the integral equations of the functional linear model components of the model. Figure 12 shows the patterns of missingness by age for the breastfeeding and illness indicator functions.

Figure 13 panels (a)-(c) visualize the variability in breastfeeding dynamics captured through our generalized functional factor analysis model by showing posterior samples of

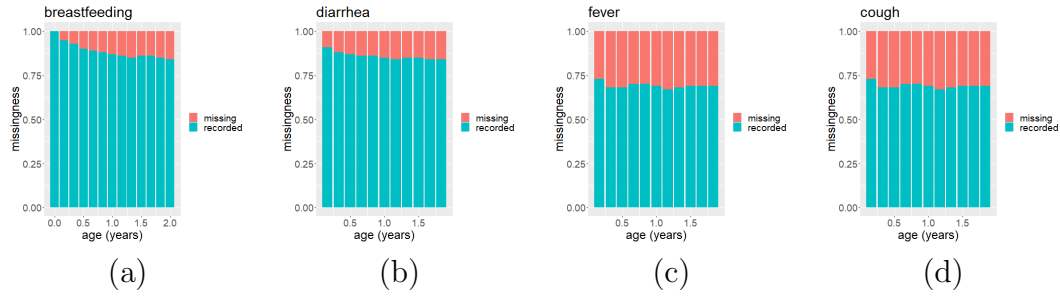


Figure 12: (a)-(d) Proportion of missing data by age for each of the binary longitudinal covariates (breastfeeding, diarrhea, fever, cough) in the Cebu Longitudinal Health and Nutritional Survey.

plus and minus one standard deviation in the direction of the generalized loadings interpreted on the probability scale through the link function  $\Phi(\cdot)$ . The loadings mostly capture if a child was breastfed at all and if so, when breastfeeding was discontinued. In the posterior samples of the mean, the values at birth are lower than at 2 months. This is due to the fact that breastfeeding status at birth was measured within the first 2 days of birth, and it could take longer than 2 days for mothers to express breast milk for the first time after childbirth (Casey et al. 1986). Panels (d)-(f) of Figure 13 shows posterior samples of underlying processes describing the probability that a child is fed breast milk by age for different subjects. In panel (d), breastfeeding status was only recorded at 4 ages (black dots). Between the ages when the child was reported to have breast milk, the model infers that the child was fed breast milk. After the last recording, the model is uncertain if and when the child stopped. In panel (e), initially the child was reported to not have breast milk, so the model infers that the child was not given breast milk after the age of the last recording. In panel (f), the child was reported to have breastfed early on, and stopped at some age after age 1. The model is uncertain when breastfeeding was discontinued.

Figure 14 shows latent factors for weight and breastfeeding status. In panel (a), the factors of weight appear much more normal, relative to the latent factors associated with breastfeeding status shown in panel (b). We investigate atypical observations for breastfeeding in Figure 15. Outliers in terms of the second factor are shown in panels (a)-(c). In general, it looks like these outliers correspond to the situation where a child was reported

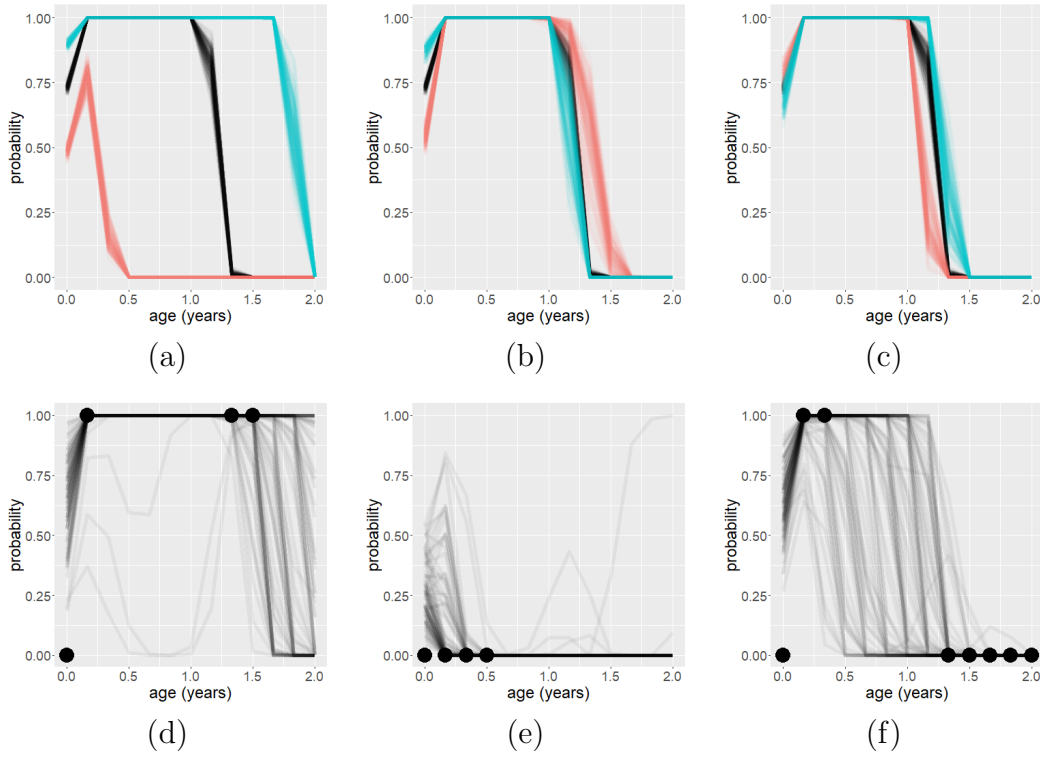


Figure 13: (a)-(c) Posterior samples of  $\Phi(\mu^{z_1}(\vec{t}))$  (black) and  $\Phi(\mu^{z_1}(\vec{t}) \pm \text{sd}(\eta_{\cdot k}^z)\lambda_k^z(\vec{t}))$  (blue and red) for  $k = 1, 2, 3$ , representing the variability described by the loadings of breastfeeding trajectories. (d)-(f) Posterior samples fitted breastfeeding trajectories,  $\Phi(\mu^{z_1}(\vec{t}) + (\lambda_1^z(\vec{t}), \lambda_2^z(\vec{t}), \lambda_3^z(\vec{t}))^\top \eta_i^z)$  overlaid on  $z_{i,1}(\vec{t}_i)$  for  $i = 250, 1079, 2087$ .

not to have breastfed erratically at an early age. Panels (d)-(f) show outliers in terms of the third factor. These outliers correspond to the situation where a child was reported not to have breastfed sometime after age 1, but continued to breastfeed after age 1.5. In addition to these outliers, the non-normal structure of the factors is replicated in exploratory data analyses presented in Section F.3.

In contrast with the breastfeeding covariates, there does not appear to be structured variability in timing of illness, with children experiencing diarrhea, fever and cough sporadically. Consequently, model based imputation is based only on a mean process interpreted on the probability scale through the link function  $\Phi(\cdot)$ . Figure 16 panels (a)-(c) show posterior samples of the average probability that a child experiences diarrhea, fever, or cough by age. Generally, children experienced fever more often than diarrhea, and cough more often than fever. In all of these mean processes, there appears to be a local maxima before



year 1. The effects on weight of experiencing these illnesses with all other variables held constant are shown in panels (d)-(f). Diarrhea tends to affect weight more than fever, and fever tends to affect weight more than cough. These regression functions tend to be more negative at higher ages. We speculate that the effects of diarrhea and fever affect weight more than cough because they can lead to dehydration (National Library of Medicine (US) 2022).

### F.3 Data Analysis using Competing Model (Crainiceanu & Goldsmith 2010)

In this section, we analyze the Cebu dataset with methods discussed in Crainiceanu & Goldsmith (2010), which we compare to the results from the NeMO model. The observation model is given by Equations (30)&(31). In line with their empirical Bayes setup,  $\mu(\vec{t})$  is estimated using the cross sectional mean of the data, and  $\lambda_1, \dots, \lambda_K$  are estimated from the mean-centered data using a penalized spline based approach. Additionally, we complete longitudinal covariates using model based imputation, with the generative model

$$P(z_{i,1}(t) = 1) = \text{logit}^{-1}(\mu^{z_1} + (\lambda_1^z(t), \dots, \lambda_{K^z}^z(t))^\top \eta_i^z),$$

$$P(z_{i,j}(t) = 1) = \text{logit}^{-1}(\mu^{z_j}), \quad j = 2, 3, 4,$$

where model components are estimated using the `slfpca` R package.

The mean of the response and loadings are fixed at point estimates,  $\hat{\mu}(\vec{t}), \hat{\lambda}_1(\vec{t}), \dots, \hat{\lambda}_K(\vec{t})$  in subsequent modeling. Remaining model parameters are assigned conjugate prior distributions and posterior inference is carried out through Gibbs sampling. As suggested by Crainiceanu & Goldsmith (2010), *a priori*  $\Theta_{k,q} \sim N(0, \hat{\phi}_k)$  and  $\xi \sim N(0, \hat{\phi}_k)$ , where the prior variances are eigenvalues of the estimated covariance matrix that determine the estimated loadings. For the regression coefficients between the scalar covariates and the latent factors, we assume independent, identically distributed standard normal priors. We use the

same bases discussed in the main paper to simplify the integral equations in the functional linear model components that govern the relationships between the longitudinal covariates and weight. Basis coefficients are given normal conjugate priors, consistent with the NeMO model.

Figure 17 panels (a) and (b) show the estimated mean process and loadings. These estimated functions are similar in shape and magnitude to the loadings presented in the main paper. Panels (d)-(f) of this figure show the inferred effects of the scalar covariates by displaying posterior samples of  $(\hat{\lambda}_1(t), \dots, \hat{\lambda}_K(t))\hat{\Theta}_q$ ,  $q = 1 \dots, 4$ . For  $q = 1, 2, 3$  the resulting functions match the results presented in the main paper. The function for  $q = 4$  in the main paper is inferred to be closer to zero with a considerable amount of uncertainty. The discrepancy between these two results could be from conditioning on estimated loadings in the empirical Bayes setting.

Figure 18 panels (a)-(c) visualize estimated generalized functional factor loadings used to describe the structure variability in breastfeeding status estimated from the `slfPCA` R package. These loadings seem to capture if a child is breastfed, and when they stopped breastfeeding. Panels (d) of this figure shows estimated latent factors,  $\hat{\eta}_i^z$ ,  $i = 1, \dots, n$ . As in Section F.2, the latent factors have a non-Gaussian structure. Panel (e)-(h) display  $\|\int_{\mathcal{T}} \hat{\beta}_1 1_{s \leq s'} ds\|_2$ , for different values of  $s'$ . The general shape of inferred functions is consistent with those presented in the main paper, however, the functions in panels (e)-(h) are slightly smaller in magnitude. As shown in panel (f), there is a diminishing effect of prolonged breastfeeding.

Figure 19 panel (a) displays the estimated average probability of a child experiencing the illnesses by age. As in the model presented in the main paper, all of these estimated functions have a prominent peak at early ages. The estimated regression functions,  $\beta_j(t)$ ,  $j = 2, 3, 4$ , shown in panels (b)-(d), match their corresponding interpretations in the main paper. It appears that experiencing diarrhea and fever have a more negative effect on weight than experiencing cough.

The inferences made in this section are generally consistent with the inferences presented

in the main paper. We use the widely applicable information criterion to compare the predictive ability of the model presented in this section and the NeMO model (Vehtari et al. 2017). The widely applicable information criterion values are  $WAIC_{NeMO} = 69709.10$  for the NeMO model and  $WAIC_{CG} = 69905.07$  for the model of Crainiceanu & Goldsmith (2010). The difference in WAICs is  $WAIC_{NeMO} - WAIC_{CG} = -195.97$  with standard error 114.04. Using this criteria, the NeMO model is preferred in terms of predictive accuracy.

## F.4 Model Fit Assessment

In this section, we assess the fit of the NeMO model to the Cebu data presented in the main paper.

Let  $f_i(\vec{t}) = \mu(\vec{t}) + (\lambda_1(\vec{t}), \dots, \lambda_K(\vec{t}))^\top \eta_i + \sum_{j=1}^4 \int_T \beta_j(s, \vec{t}) z_{i,j}(s) ds$  denote the function that underlies the sparse and noisy observation  $y_i(\vec{t}_i)$ ,  $f_i^{[iter]}(\vec{t})$  denote posterior Markov chain Monte Carlo samples, and let  $\hat{f}_i(\vec{t})$  denote the posterior mean computed from Markov chain Monte Carlo samples. Residuals are estimated as  $\hat{\epsilon}_i(\vec{t}_i) = y_i(\vec{t}_i) - \hat{f}_i(\vec{t}_i)$ . Figure 21 shows a boxplot of estimated residuals for all subjects,  $i = 1, \dots, n$ , by age. Visually, it appears that there is no mean trend across ages, and there does not appear to be substantial heteroskedasticity.

We further assess the fit of the model using posterior predictive checks (Gelman et al. 2013). Under the assumed model, posterior predictive samples are generated via  $y_i^{pred, [iter]}(\vec{t}_i) \sim N(f_i^{[iter]}, \sigma^{[iter], 2} I_{m_i})$ . Quantities of interest,  $T$ , based on the posterior predictive samples are compared to the same quantities computed using the actual observations. We consider the following quantities of interest used to study the fit of our model,

$$\begin{aligned} T_{mag, y_i} &= \|y_i\|_2, \quad i = 1, \dots, n \\ T_{mean, (y_1, \dots, y_n)}(t) &= \frac{1}{n} \sum_{i=1}^n y_i(t), \quad t = 0, \frac{2}{24}, \dots, 2 \\ T_{var, (y_1, \dots, y_n)}(k) &= \text{eig}_k \left( \text{cov}(y(s), y(t)) \right), \quad k = 1 \dots, K, \end{aligned}$$

where  $\text{eig}_k$  denotes the  $k^{\text{th}}$  largest eigenvalue of the sample covariance matrix based on  $y_1, \dots, y_n$ . The quantity  $T_{mag}$  can be used to assess how well the model captures the magnitude of individual subjects,  $T_{mean}$  can be used to assess how well the model captures the mean trend across subjects, and  $T_{var}$  can be used to assess how well the modes of variability are captured across subjects.

Figure 22 panels (a)-(f) show histograms of  $T_{mag,y_i}$  based on posterior predictive draws for different subjects, where the red line represents  $T_{mag,y_i}$  based on actual observed values. Panels (a)-(c) represent random samples of subjects in the population, while panels (d)-(f) represent subjects having posterior predictive mean of  $T_{mag,y_i}$  furthest from the observed value. Even in the worst case scenario, the predictions based on the model cover the observed value. Panel (g) of this figure shows a histogram of the absolute difference between the mean of  $T_{mag,y_i}$  based on posterior predictive samples and the observed value. The absolute difference is mostly concentrated near zero. Figure 23 panels (a)-(f) show histograms of  $T_{mean,(y_1,\dots,y_n)}$  based on posterior predictive draws at different times  $t = 0, \dots, 2$ , where the red line represents  $T_{mean,(y_1,\dots,y_n)}$  based on actual observed values. These values are computed cross-sectionally by removing missing values. At each time, it appears that the observed value of  $T_{mean,(y_1,\dots,y_n)}$  is covered by the values computed using posterior predictive samples. Figure 24 panels (a)-(f) show histograms of  $T_{var,(y_1,\dots,y_n)}$  based on posterior predictive draws for different eigenvalues  $k = 1, \dots, 5$ , where the red line represents  $T_{var,(y_1,\dots,y_n)}$  based on actual observed values. The sample covariance is computed by using pairwise complete observations. For each eigenvalue the observed value of  $T_{var,(y_1,\dots,y_n)}$  is covered by the values computed using posterior predictive samples. Based on these posterior predictive checks, it is apparent that the model is adequate in describing these individual and population level features of the observations.

In the main paper, cough, season, and strata are noted as the covariates with the smallest effect on the response. We consider reducing the model presented in the main paper by omitting these covariates. In order to assess fit of reduced models, compared to a full model with all covariates, we use widely applicable information criterion. Results are

Table 1: Widely applicable information criterion (WAIC) for full versus reduced models. In all cases the full model is preferred.

covariate omitted	WAIC	difference (full - reduced)	standard error (difference in WAIC)
cough	69727.66	-18.40	26.41
season	69719.45	-10.19	33.76
strata	69718.37	-9.11	26.41

presented in Table 1. For each case, the full model is preferred.

## F.5 Markov chain Monte Carlo Trace Plots

The inferential results of the main paper are based on Markov chain Monte Carlo samples. In this section we plot thinned Markov chain Monte Carlo samples to diagnose convergence. The diagnostic plots for all parameters do not indicate that there is an issue with Markov chain Monte Carlo convergence. Figure 25 displays trace plots related to the inferential results of Figures 7&12 of the main paper. Figure 26 displays trace plots related to the inferential results of Figure 8 of the main paper. Figure 27 displays trace plots related to the inferential results of Figures 9&10 of the main paper. Figure 28 displays trace plots related to the inferential results of Figures 11 of the main paper

## References

- Adair, L., Popkin, B. M., VanDerslice, J., Akin, J., Guilkey, D., Black, R., Briscoe, J. & Flieger, W. (1993), ‘Growth dynamics during the first two years of life: A prospective study in the Philippines’, *European Journal of Clinical Nutrition* **47**(1), 42–51.
- Adair, L. S. & Guilkey, D. K. (1997), ‘Age-specific determinants of stunting in Filipino children’, *The Journal of Nutrition* **127**(2), 314–320.
- Adair, L. S., Popkin, B. M., Akin, J. S., Guilkey, D. K., Gultiano, S., Borja, J., Perez, L.,

- Kuzawa, C. W., McDade, T. & Hindin, M. J. (2011), ‘Cohort profile: The Cebu longitudinal health and nutrition survey’, *International Journal of Epidemiology* **40**(3), 619–625.
- Albert, J. H. & Chib, S. (1993), ‘Bayesian analysis of binary and polychotomous response data’, *Journal of the American Statistical Association* **88**(422), 669–679.
- Andrieu, C. & Thoms, J. (2008), ‘A tutorial on adaptive MCMC’, *Statistics and Computing* **18**(4), 343–373.
- Behseta, S., Kass, R. E. & Wallstrom, G. L. (2005), ‘Hierarchical models for assessing variability among functions’, *Biometrika* **92**(2), 419–434.
- Bhattacharya, A. & Dunson, D. B. (2011), ‘Sparse Bayesian infinite factor models’, *Biometrika* **98**(2), 291–306.
- Casey, C. E., Neifert, M. R., Seacat, J. M. & Neville, M. C. (1986), ‘Nutrient intake by breast-fed infants during the first five days after birth’, *American Journal of Diseases of Children* **140**(9), 933–936.
- Crainiceanu, C. M. & Goldsmith, A. J. (2010), ‘Bayesian functional data analysis using WinBUGS’, *Journal of Statistical Software* **32**(11), 1–33.
- Dasgupta, S., Pati, D., Jermyn, I. H. & Srivastava, A. (2021), ‘Modality-constrained density estimation via deformable templates’, *Technometrics* **63**(4), 536–547.
- Dewey, K. G. (1998), ‘Growth characteristics of breast-fed compared to formula-fed infants’, *Neonatology* **74**(2), 94–105.
- Duan, L. L., Young, A. L., Nishimura, A. & Dunson, D. B. (2019), ‘Bayesian constraint relaxation’, *Biometrika* **107**(1), 191–204.
- Earls, C. & Hooker, G. (2017), ‘Combining functional data registration and factor analysis’, *Journal of Computational and Graphical Statistics* **26**(2), 296–305.

- Ferraty, F. & Vieu, P. (2006), *Nonparametric Functional Data Analysis: Theory and Practice*, Springer.
- Gelman, A., Carlin, J. B., Stern, H. S., Dunson, D. B., Vehtari, A. & Rubin, D. B. (2013), *Bayesian Data Analysis*, Chapman and Hall/CRC.
- Ghosh, J. & Dunson, D. B. (2009), ‘Default prior distributions and efficient posterior computation in Bayesian factor analysis’, *Journal of Computational and Graphical Statistics* **18**(2), 306–320.
- Goldsmith, J., Zipunnikov, V. & Schrack, J. (2015), ‘Generalized multilevel function-on-scalar regression and principal component analysis’, *Biometrics* **71**(2), 344–353.
- Hall, P., Müller, H.-G. & Yao, F. (2008), ‘Modelling sparse generalized longitudinal observations with latent Gaussian processes’, *Journal of the Royal Statistical Society: Series B* **70**(4), 703–723.
- Hannah, L. A. & Dunson, D. B. (2013), ‘Multivariate convex regression with adaptive partitioning’, *The Journal of Machine Learning Research* **14**(1), 3261–3294.
- Harville, D. A. (1998), *Matrix Algebra from a Statistician’s Perspective*, Springer.
- Hastie, T. & Tibshirani, R. (1993), ‘Varying-coefficient models’, *Journal of the Royal Statistical Society: Series B* **55**(4), 757–779.
- Hodges, J. S. & Reich, B. J. (2010), ‘Adding spatially-correlated errors can mess up the fixed effect you love’, *The American Statistician* **64**(4), 325–334.
- James, G. M., Hastie, T. J. & Sugar, C. A. (2000), ‘Principal component models for sparse functional data’, *Biometrika* **87**(3), 587–602.
- Jauch, M., Hoff, P. D. & Dunson, D. B. (2021), ‘Monte Carlo simulation on the Stiefel manifold via polar expansion’, *Journal of Computational and Graphical Statistics* **30**(3), 622–631.

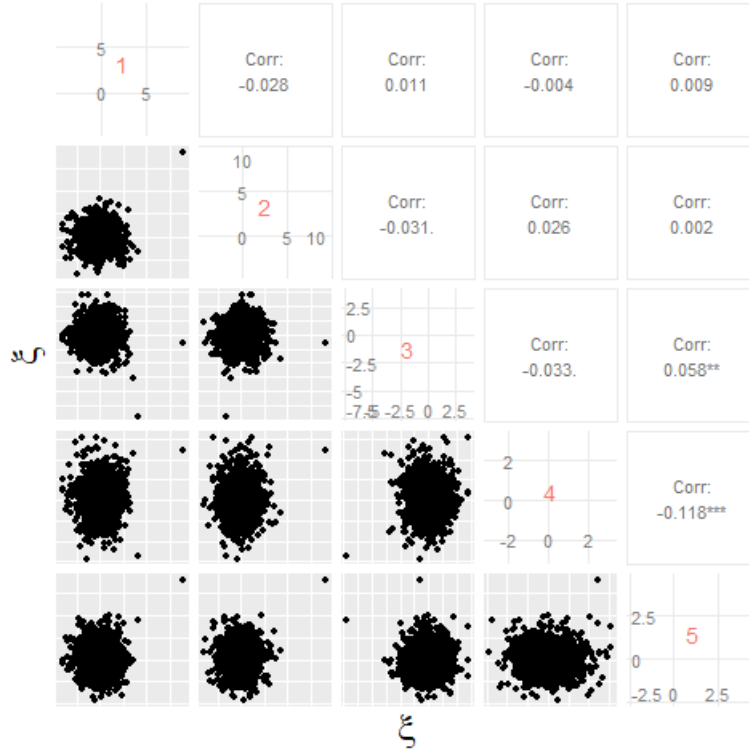
- Jiang, L., Zhong, Y., Elrod, C., Natarajan, L., Knight, R. & Thompson, W. K. (2020), ‘Bayestime: Bayesian functional principal components for sparse longitudinal data’, arXiv:2012.00579.
- Khan, K. & Calder, C. A. (2022), ‘Restricted spatial regression methods: Implications for inference’, *Journal of the American Statistical Association* **117**(537), 482–494.
- Kneip, A. & Ramsay, J. O. (2008), ‘Combining registration and fitting for functional models’, *Journal of the American Statistical Association* **103**(483), 1155–1165.
- Kowal, D. R. (2021), ‘Dynamic regression models for time-ordered functional data’, *Bayesian Analysis* **16**(2), 459 – 487.  
**URL:** <https://doi.org/10.1214/20-BA1213>
- Kowal, D. R. & Canale, A. (2021), ‘Semiparametric functional factor models with Bayesian rank selection’, arXiv:108.02151.
- Kowal, D. R., Matteson, D. S. & Ruppert, D. (2017), ‘A Gaussian multivariate functional dynamic linear model’, *Journal of the American Statistical Association* **112**(518), 733–744.
- Lenk, P. J. & Choi, T. (2017), ‘Bayesian analysis of shape-restricted functions using Gaussian process priors’, *Statistica Sinica* pp. 43–69.
- Lin, L. & Dunson, D. B. (2014), ‘Bayesian monotone regression using Gaussian process projection’, *Biometrika* **101**(2), 303–317.
- Malfait, N. & Ramsay, J. O. (2003), ‘The historical functional linear model’, *Canadian Journal of Statistics* **31**(2), 115–128.
- Marco, N., Şentürk, D., Jeste, S., DiStefano, C., Dickinson, A. & Telesca, D. (2022), ‘Functional mixed membership models’, arXiv:2206.12084.



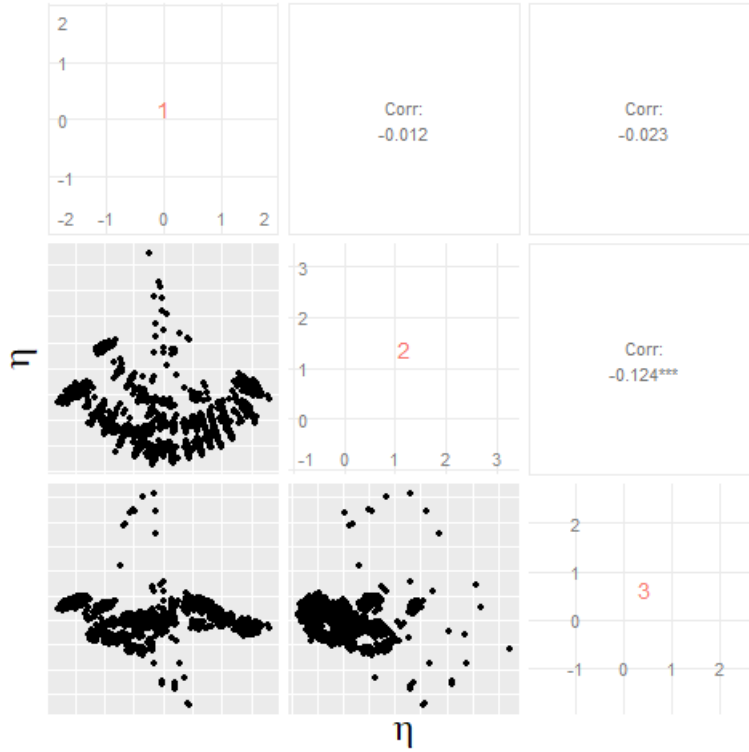
- Marcus, M. B. & Shepp, L. A. (1972), Sample behavior of Gaussian processes, *in* ‘Proceedings of the Sixth Berkeley Symposium on Mathematics, Statistics and Probability’, Vol. 2, pp. 423–421.
- Marron, J. S., Ramsay, J. O., Sangalli, L. M. & Srivastava, A. (2015), ‘Functional data analysis of amplitude and phase variation’, *Statistical Science* **30**(4), 468–484.
- Montagna, S., Tokdar, S. T., Neelon, B. & Dunson, D. B. (2012), ‘Bayesian latent factor regression for functional and longitudinal data’, *Biometrics* **68**(4), 1064–1073.
- Moran, K. R., Dunson, D., Wheeler, M. W. & Herring, A. H. (2021), ‘Bayesian joint modeling of chemical structure and dose response curves’, *The Annals of Applied Statistics* **15**(3), 1405–1430.
- National Library of Medicine (US) (2022), ‘Dehydration’, MedlinePlus. URL: <https://medlineplus.gov/dehydration.html>.
- Nolan, T. H., Goldsmith, J. & Ruppert, D. (2021), ‘Bayesian functional principal components analysis via variational message passing’, arXiv:2104.00645.
- Peng, J. & Paul, D. (2009), ‘A geometric approach to maximum likelihood estimation of the functional principal components from sparse longitudinal data’, *Journal of Computational and Graphical Statistics* **18**(4), 995–1015.
- Plumlee, M. & Joseph, V. R. (2018), ‘Orthogonal Gaussian process models’, *Statistica Sinica* **28**(2), 601–619.
- Poworoznek, E., Ferrari, F. & Dunson, D. (2021), ‘Efficiently resolving rotational ambiguity in Bayesian matrix sampling with matching’, arXiv:2107.13783.
- Ramsay, J. O. & Dalzell, C. (1991), ‘Some tools for functional data analysis’, *Journal of the Royal Statistical Society: Series B* **53**(3), 539–561.
- Ramsay, J. & Silverman, B. (2005), *Functional Data Analysis*, Springer Series in Statistics, Springer.

- Resnick, S. (2019), *A Probability Path*, Springer.
- Ruppert, D., Wand, M. P. & Carroll, R. J. (2003), *Semiparametric regression*, Cambridge University Press.
- Schiavon, L., Canale, A. & Dunson, D. B. (2022), ‘Generalized infinite factorization models’, *Biometrika* **109**(3), 817–835.  
**URL:** <https://doi.org/10.1093/biomet/asab056>
- Shamshoian, J., Şentürk, D., Jeste, S. & Telesca, D. (2022), ‘Bayesian analysis of longitudinal and multidimensional functional data’, *Biostatistics* **23**(2), 558–573.
- Shively, T. S., Sager, T. W. & Walker, S. G. (2009), ‘A Gaussian approach to non-parametric monotone function estimation’, *Journal of the Royal Statistical Society: Series B* **71**(1), 159–175.
- Shively, T. S., Walker, S. G. & Damien, P. (2011), ‘Nonparametric function estimation subject to monotonicity, convexity and other shape constraints’, *Journal of Econometrics* **161**(2), 166–181.
- Suarez, A. J. & Ghosal, S. (2017), ‘Bayesian estimation of principal components for functional data’, *Bayesian Analysis* **12**(2), 311 – 333.
- Tipping, M. E. & Bishop, C. M. (1999), ‘Probabilistic principal component analysis’, *Journal of the Royal Statistical Society: Series B* **61**(3), 611–622.
- van der Linde, A. (2008), ‘Variational Bayesian functional PCA’, *Computational Statistics & Data Analysis* **53**, 517–533.
- van der Linde, A. (2009), ‘A Bayesian latent variable approach to functional principal components analysis with binary and count data’, *AStA Advances in Statistical Analysis* **93**(3), 307–333.

- van Zanten, J. & van der Vaart, A. (2008), Reproducing kernel Hilbert spaces of Gaussian priors, *in* ‘Pushing the Limits of Contemporary Statistics: Contributions in Honor of Jayanta K. Ghosh’, Institute of Mathematical Statistics.
- Vehtari, A., Gelman, A. & Gabry, J. (2017), ‘Practical Bayesian model evaluation using leave-one-out cross-validation and WAIC’, *Statistics and Computing* **27**(5), 1413–1432.
- Wheeler, M. W., Dunson, D. B. & Herring, A. H. (2017), ‘Bayesian local extremum splines’, *Biometrika* **104**(4), 939–952.
- Wrobel, J., Zipunnikov, V., Schrack, J. & Goldsmith, J. (2019), ‘Registration for exponential family functional data’, *Biometrics* **75**(1), 48–57.
- Yao, F., Müller, H.-G. & Wang, J.-L. (2005), ‘Functional data analysis for sparse longitudinal data’, *Journal of the American Statistical Association* **100**(470), 577–590.
- Yu, C.-H., Li, M., Noe, C., Fischer-Baum, S. & Vannucci, M. (2022), ‘Bayesian inference for stationary points in Gaussian process regression models for event-related potentials analysis’, *Biometrics* .
- Zhong, R., Liu, S., Li, H. & Zhang, J. (2021), ‘Sparse logistic functional principal component analysis for binary data’, arXiv:2109.08009.



(a)



(b)

Figure 14: Scatter plot matrices of posterior means of latent factors for (a)  $\xi$  (weight) and (b)  $\eta^z$  (breastfeeding).

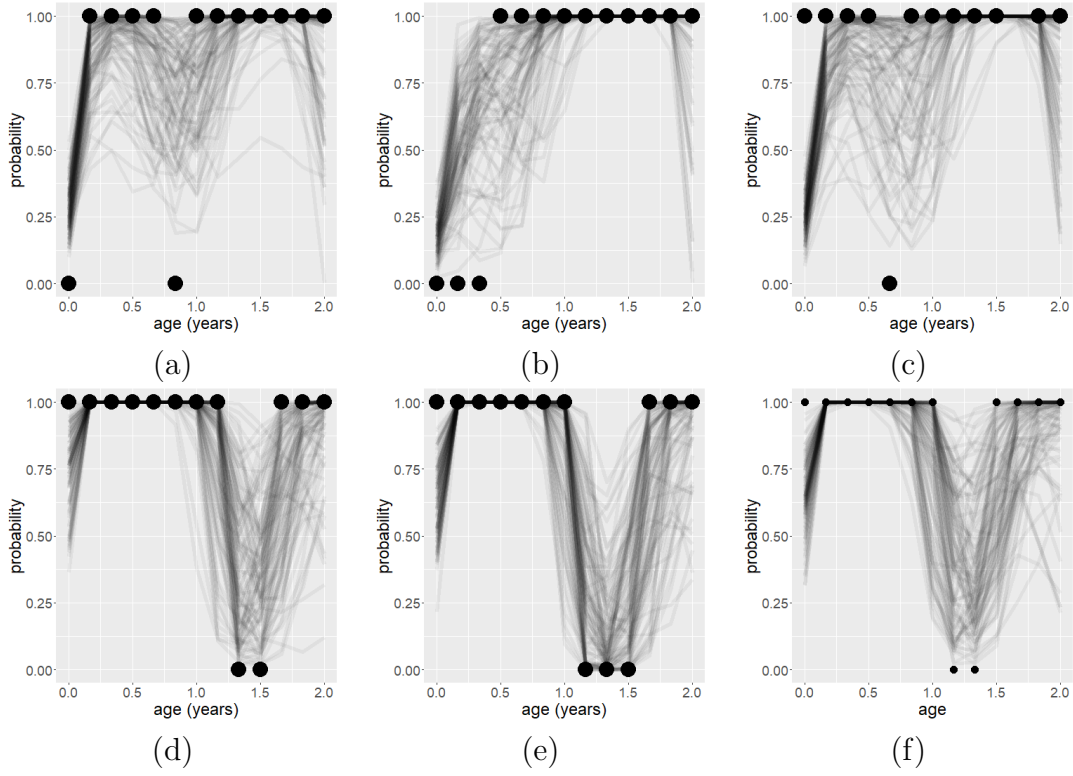


Figure 15: (a)-(f) Posterior samples of fitted atypical breastfeeding trajectories,  $\Phi(\mu^{z_1}(\vec{t}) + (\lambda_1^z(\vec{t}), \lambda_2^z(\vec{t}), \lambda_3^z(\vec{t}))^\top \eta_i^z)$  overlaid on  $z_{i,1}(\vec{t}_i)$  for  $i = 212, 2782, 2809, 1516, 1844, 2701$ .

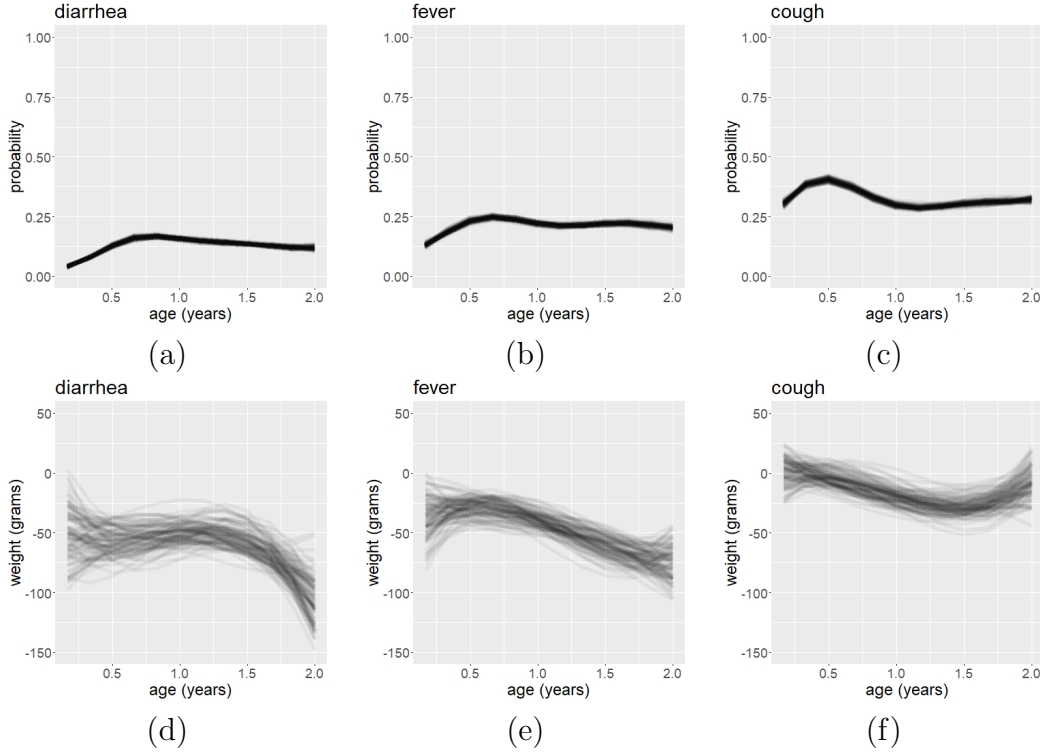


Figure 16: (a)-(c) Posterior samples of  $\Phi(\mu^{z_j}(\vec{t}))$  for  $j = 2, 3, 4$ , representing the proportion of children in the study that experienced an illness by age. (d)-(f) Posterior samples of  $\beta_j(\vec{t})$ ,  $j = 2, 3, 4$ , representing the effect of experiencing an illness on weight. Children tend to experience cough more often than fever and fever more often than diarrhea. Experiencing diarrhea or fever tend to have a larger effect on weight than experiencing cough.

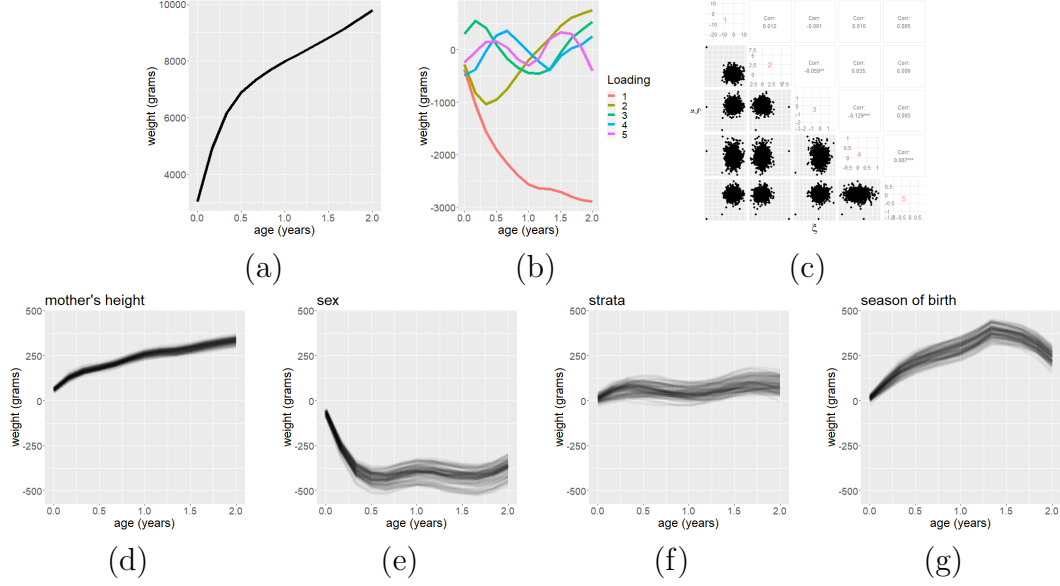


Figure 17: Inferred parameters related to functional factor analysis of weight and scalar covariates using the model of Crainiceanu & Goldsmith (2010): (a)  $\hat{\mu}(t)$ . (b)  $\sqrt{\hat{\psi}_1} \hat{\lambda}_1, \dots, \sqrt{\hat{\psi}_K} \hat{\lambda}_K$ . (c) Posterior means of  $\xi_{i,k}$   $i = 1, \dots, n$   $k = 1, \dots, K$ . (d)-(g) Posterior samples of  $(\hat{\lambda}_1(t), \dots, \hat{\lambda}_K(t)) \Theta_q$ ,  $q = 1 \dots, 4$ .

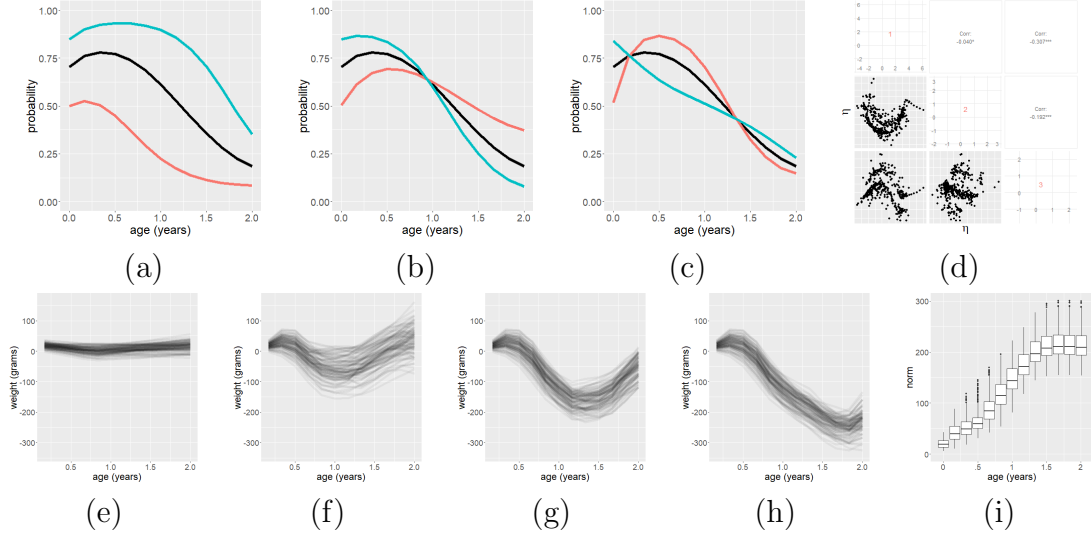


Figure 18: Inference for parameters related to modeling breastfeeding status on weight using the Crainiceanu & Goldsmith (2010) model: (a)-(c)  $\text{logit}^{-1}(\hat{\mu}^{z_1} \pm \text{sd}(\hat{\eta}_{1,k}^z, \dots, \hat{\eta}_{n,k}^z) \hat{\lambda}_k^z(t))$  for  $k = 1, 2, 3$ . (d) latent factors,  $\eta_{i,k}^z$   $i = 1, \dots, n$ ,  $k = 1, 2, 3$ . (e)-(h) Posterior samples of  $\int_{\mathcal{T}} \beta_1 1_{s \leq s'} ds$   $s' = 0, 0.5, 1, 2$ . (i) Boxplots of posterior samples of  $\|\int_{\mathcal{T}} \hat{\beta}_1 1_{s \leq s'} ds\|_2$  for different values of  $s'$ .

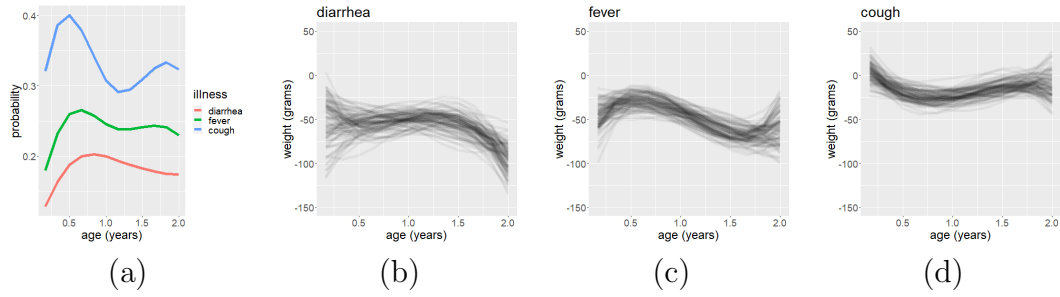


Figure 19: Inferred functions related to modelling the effects of illness on weight using the Crainiceanu & Goldsmith (2010) model: (a)  $\text{logit}^{-1}(\hat{\mu}^{z_j}(t))$ . (b)-(d) Posterior samples of  $\beta_j(t)$  for  $j = 2, 3, 4$ .

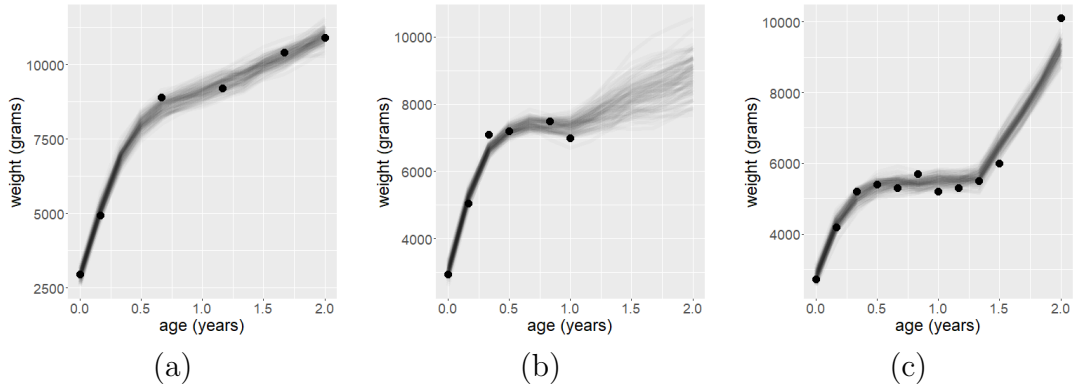


Figure 20: Inferred weight trajectories for different subjects using the Crainiceanu & Goldsmith (2010) model: (a)-(c) Posterior samples of  $\hat{\mu}(\vec{t}_i) + (\hat{\lambda}_1(\vec{t}_i), \dots, \hat{\lambda}_K(\vec{t}_i))^\top \hat{\eta}_i + O_i \sum_{j=1}^4 \int_T \beta_j(s, \vec{t}) z_{i,j}(s) ds$ , overlaid on  $y_i(\vec{t}_i)$ ,  $i = 421, 1626, 2205$ .

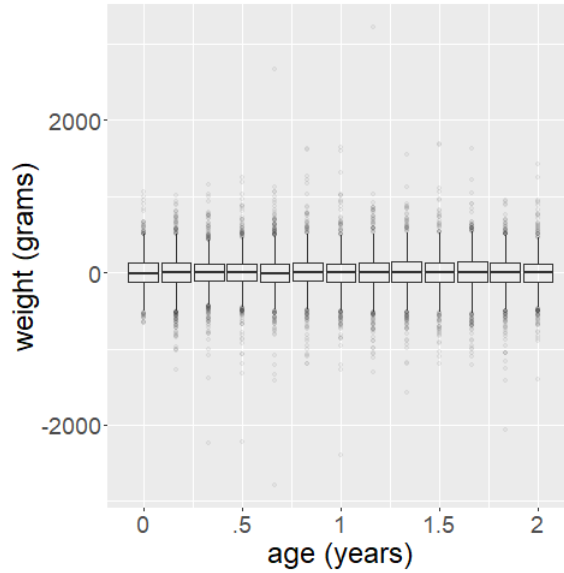


Figure 21: Boxplots of residuals by age.



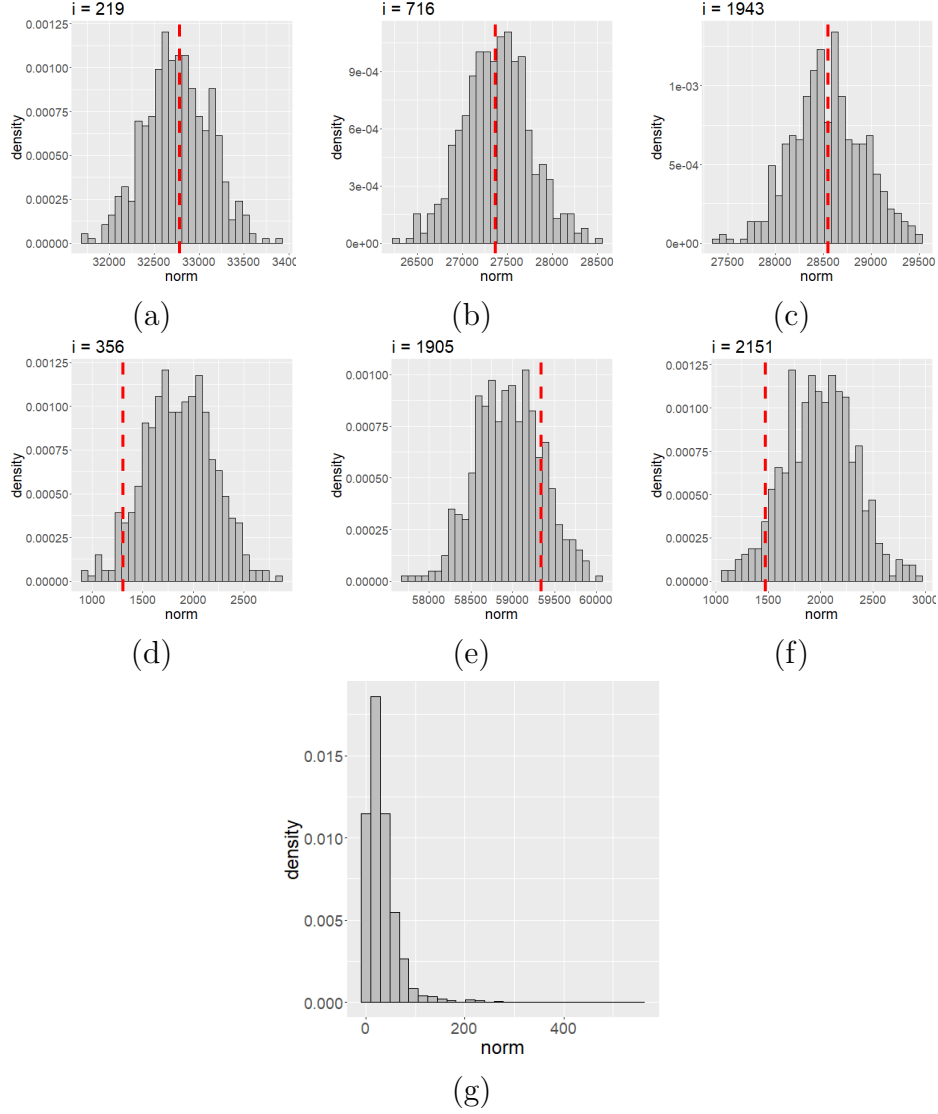


Figure 22:  $T_{mag,y_i}$  based on posterior predictive samples (histogram) and observation (red lines) for random subjects (a)-(c) and subjects whose predicted values were furthest from the observed values (d)-(f). (g) the absolute difference between the mean of  $T_{mag,y_i}$  based on posterior predictive samples and the observed value for all subjects.

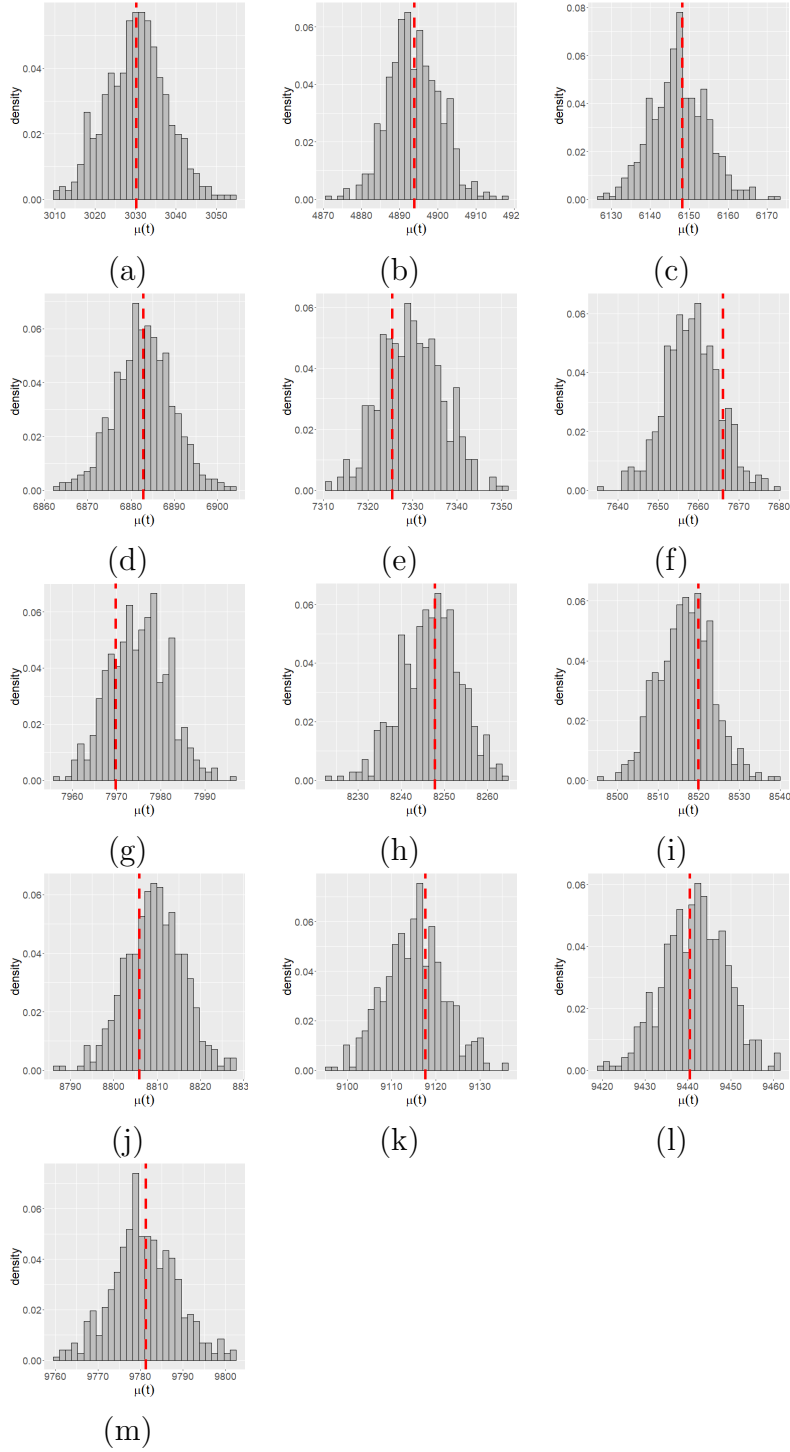


Figure 23:  $T_{mean, (y_1, \dots, y_n)}$  based on posterior predictive samples (histogram) and observation (red lines) for (a)  $t = 0$  years, (b)  $t = 2/24$  years, ..., (m)  $t = 2$  years.

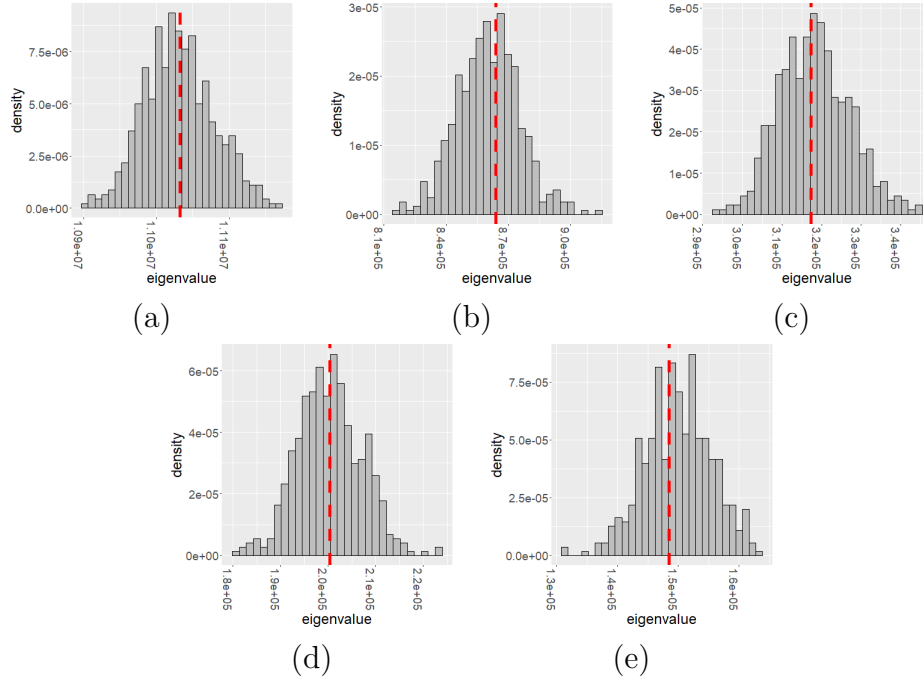


Figure 24:  $T_{var,(y_1,\dots,y_n)}$  based on posterior predictive samples (histogram) and observation (red lines) for (a)  $k = 1$ , (b)  $k = 2$ , ..., (e)  $k = 5$ .

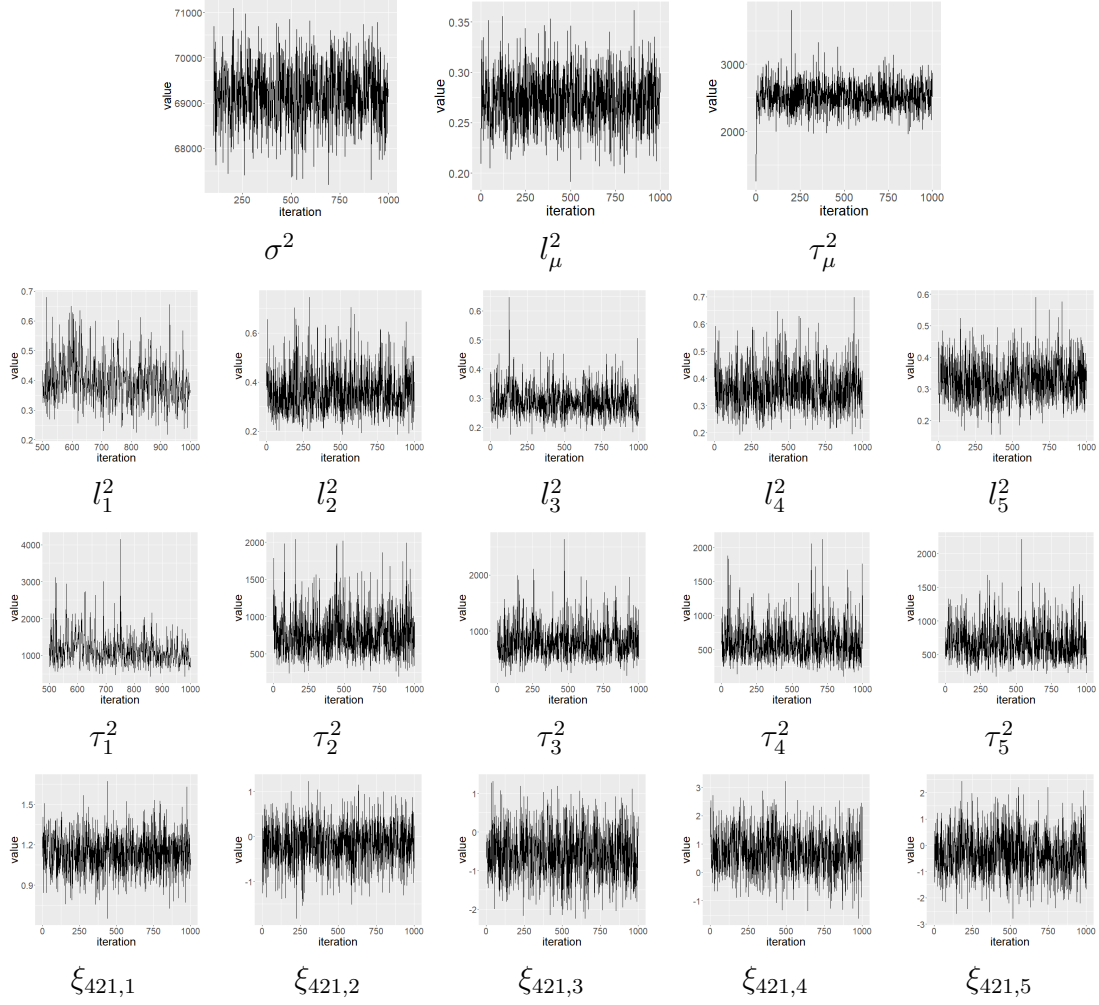


Figure 25: Trace plots related to the functional factor analysis results presented Figures 7&12 in the main paper.

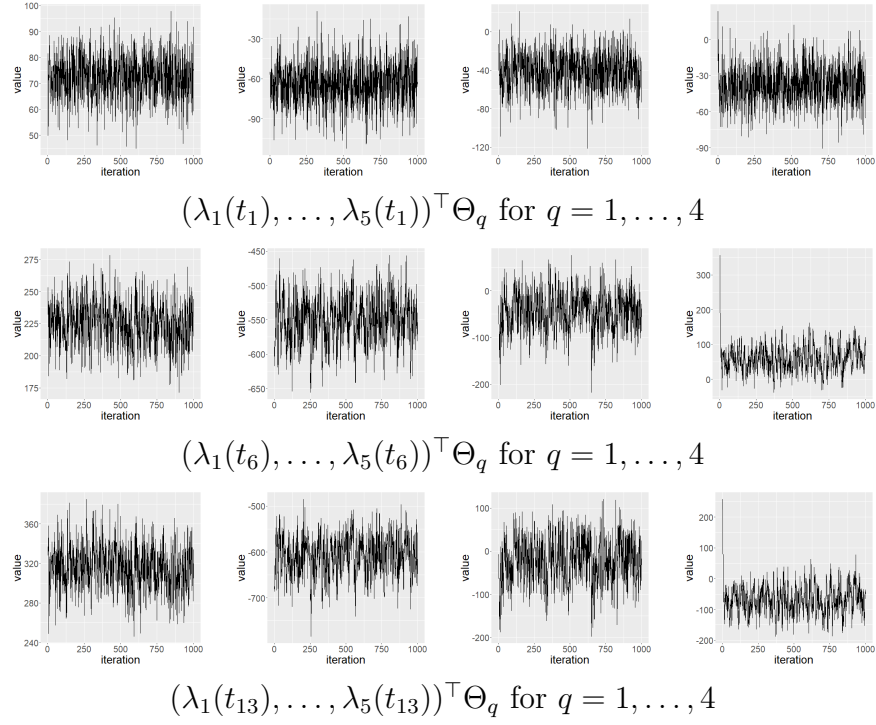


Figure 26: Trace plots related to latent factor regression onto scalar covariates presented in Figure 8 in the main paper.

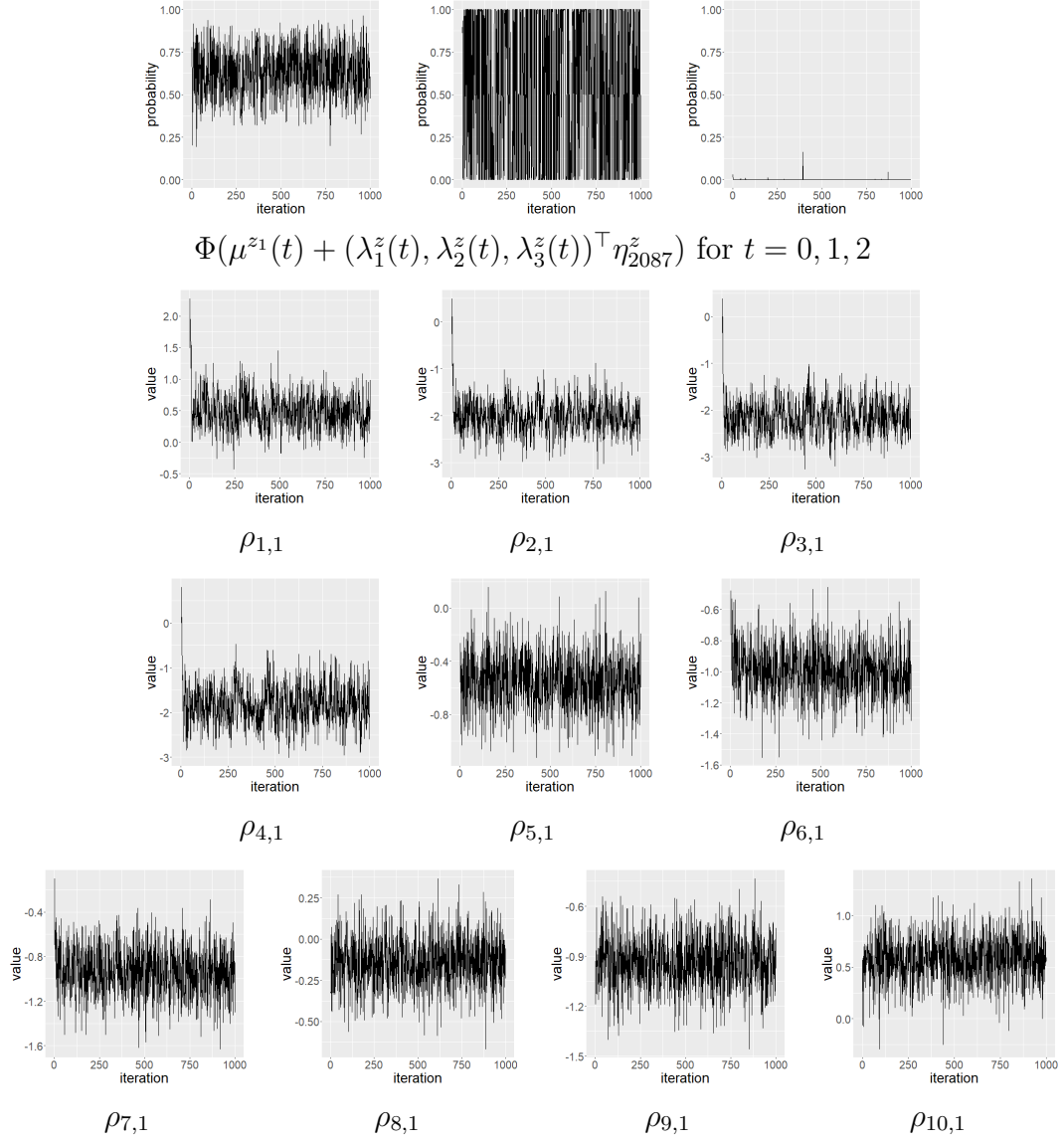


Figure 27: Trace plots related to breastfeeding status interpolation and historical regression presented in Figures 9&10 in the main paper.

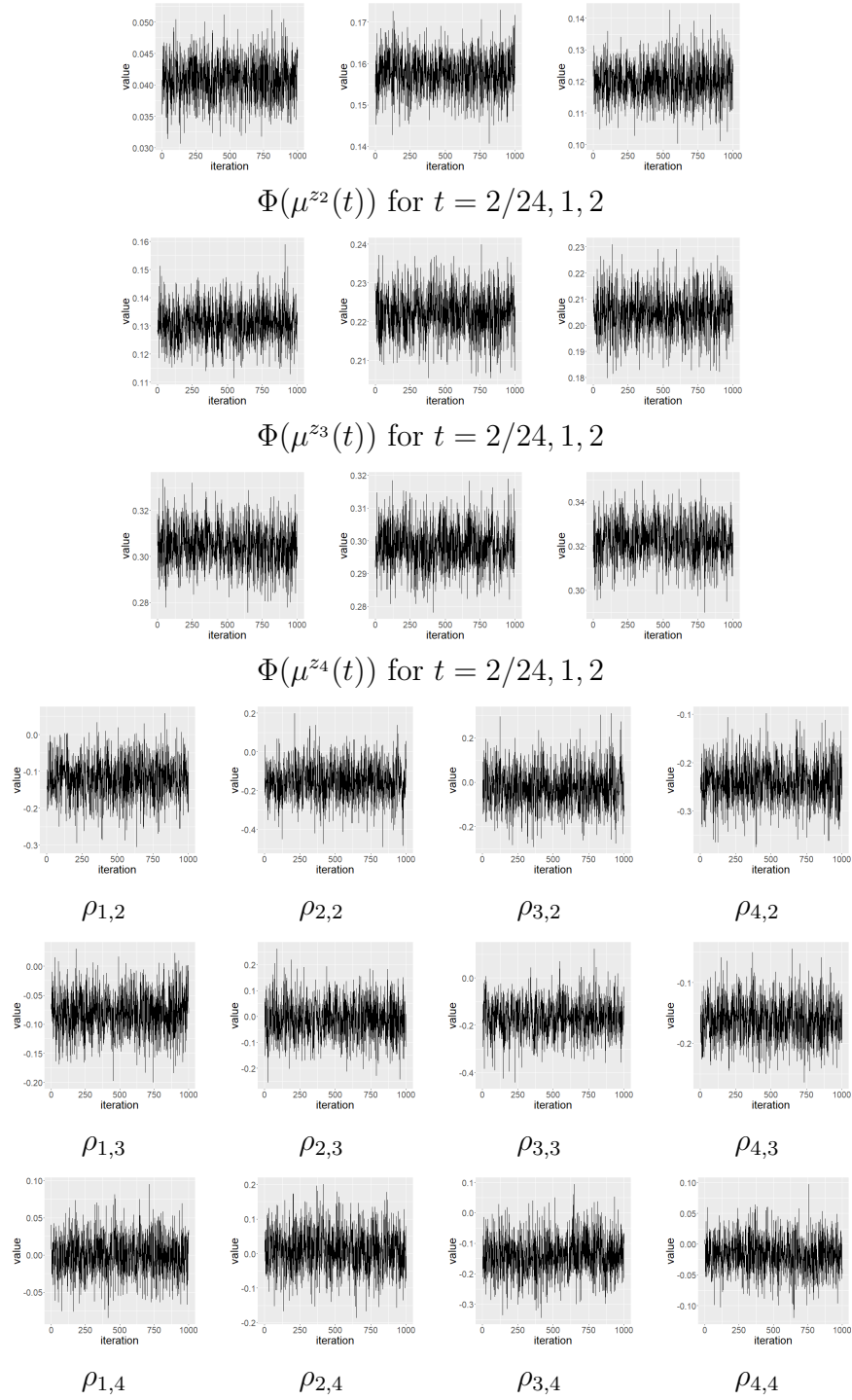


Figure 28: Trace plots related to illness status interpolation and concurrent regression presented in Figure 11 in the main paper.